

## Mismatch Effects and its Mitigation Techniques in the Solar Photovoltaic System

Niazi, Kamran Ali Khan

DOI (link to publication from Publisher):  
[10.54337/aau451017379](https://doi.org/10.54337/aau451017379)

Publication date:  
2021

Document Version  
Publisher's PDF, also known as Version of record

[Link to publication from Aalborg University](#)

Citation for published version (APA):  
Niazi, K. A. K. (2021). *Mismatch Effects and its Mitigation Techniques in the Solar Photovoltaic System*. Aalborg Universitetsforlag. <https://doi.org/10.54337/aau451017379>

### General rights

Copyright and moral rights for the publications made accessible in the public portal are retained by the authors and/or other copyright owners and it is a condition of accessing publications that users recognise and abide by the legal requirements associated with these rights.

- Users may download and print one copy of any publication from the public portal for the purpose of private study or research.
- You may not further distribute the material or use it for any profit-making activity or commercial gain
- You may freely distribute the URL identifying the publication in the public portal -

### Take down policy

If you believe that this document breaches copyright please contact us at [vbn@aub.aau.dk](mailto:vbn@aub.aau.dk) providing details, and we will remove access to the work immediately and investigate your claim.



# **MISMATCH EFFECTS AND THEIR MITIGATION TECHNIQUES IN THE SOLAR PHOTOVOLTAIC SYSTEM**

**BY  
KAMRAN ALI KHAN NIAZI**

DISSERTATION SUBMITTED 2021



**AALBORG UNIVERSITY**  
DENMARK



---

---

# **Mismatch Effects and their Mitigation Techniques in the Solar Photovoltaic System**

---

---

Ph.D. Dissertation

Kamran Ali Khan Niazi

A Dissertation Submitted to the Faculty of Engineering and Science at  
Aalborg University in Partial Fulfilment for the Degree of Doctor of  
Philosophy in Electrical Engineering

Dissertation submitted May, 2021.

Dissertation submitted: May 2021

PhD supervisors: Prof. Yongheng Yang  
Zhejiang University, Hangzhou, China  
Assoc. Prof. Tamas Kerekes  
Aalborg University, Aalborg, Denmark

Assistant PhD supervisor: Assoc. Prof. Dezso Sera  
Queensland University of Technology, Brisbane, QLD,  
Australia

PhD committee: Associate Professor Kaiyuan Lu (chair)  
Aalborg University  
Professor Dr.-Ing Jens Schneider  
Hochschule für Technik, Wirtschaft und Kultur  
Leipzig Fakultät Ingenieurwissenschaften  
Professor George Georghiou  
University of Cyprus

PhD Series: Faculty of Engineering and Science, Aalborg University

Department: Department of Energy Technology

ISSN (online): 2446-1636  
ISBN (online): 978-87-7210-962-6

Published by:  
Aalborg University Press  
Kroghstræde 3  
DK – 9220 Aalborg Ø  
Phone: +45 99407140  
aauf@forlag.aau.dk  
forlag.aau.dk

© Copyright: Kamran Ali Khan Niazi

Printed in Denmark by Rosendahls, 2021

# Abstract

The installed capacity of solar photovoltaic (PV) systems is continuously increasing due to decreasing costs and increasing environmental concerns. The energy obtained from the solar PV systems is clean and green energy. However, it is highly affected by the non-ideal environmental conditions, e.g., partial shading. These non-ideal conditions lead to a mismatch in the electrical characteristics of the solar PV system, which is built up of few to thousands of PV panels in series and parallel to achieve a specific system requirement. Due to mismatch, the entire PV system performance is affected along with the system life, which is degraded due to the stresses generated by the mismatch in the PV system.

To analyze, diagnose, and mitigate the effect of mismatch in the solar PV system, this Ph.D. study is divided into two parts. In the first part, crystalline-silicon (c-Si) and thin-film solar PV panels technologies are considered to analyze them by using infrared thermography, temperature measurement, and power-voltage (P-V) characteristics under various mismatch conditions. Additionally, infrared thermographic images are also used in the diagnoses of the mismatch effect through a machine-learning (ML)-based algorithm, i.e., Naive Bayes (nBayes) classifier. The ML classifier is used to detect the hotspots in c-Si PV panels. The developed algorithm categorizes the PV panel's infrared images into three various categories, e.g., normal, defective, and hotspot. The method achieves an efficiency above 94%.

In the second part, the techniques based on power electronics have been developed to reduce the impact of mismatch in a solar PV system. The developed techniques use smart bypass diodes and distributed power electronic topologies focusing on differential power processing (DPP) techniques to reduce the impact of mismatch. The developed topologies improve the extraction of energy from the system by reducing the stresses over the components in the topology by minimizing the peak-peak mismatch current ripples, better voltage equalization, and improving the performance under severe mismatch conditions as compare to already existed solutions. Additionally, the DPP processes only a small part (mismatched power) of power instead of processing a complete power. Hence, the size of the DPP converters is small therefore, they can easily be integrated into a PV panel junction box. Moreover, the DPP converters eliminate the multiple power peaks (MPPs) issue in the solar PV system, which reduces the complexity for maximum power point tracking (MPPT) algorithms. The proposed topologies are analyzed through simulation and experimentation. Additionally, the DPP converter along with DC optimizer is also compared with state-of-the-art solution, i.e., bypass diode technique under various mismatch scenarios to analyze the effectiveness and performance of these three techniques.

In continuation, the Ph.D. study also explores the integration of DPP topologies on various PV string interconnection schemes, e.g., series-parallel (SP), total-cross-tied (TCT), bridge-linked (BL), and central-cross-tied (CCT), to analyze their applicability on them. For this purpose, a system of 4x4 PV array is considered for analysis under various mismatched conditions. The results show that the DPP converters are only applicable to SP and CCT connections due to the inherent DPP converter structure. However, the integration with SP and CCT shows an improvement in overall energy yield. Thus, the integration of DPP with various integration schemes may be a promising solution to enhance the performance and efficiency of large PV systems.



# Abstrakt

Den installerede kapacitet på solcelleanlæg (PV) stiger kontinuerligt på grund af faldende omkostninger og stigende miljøhensyn. Den energi, der opnås fra solcelleanlæggene, er ren og grøn energi. Imidlertid er det stærkt påvirket af de ikke-ideelle miljøforhold, f.eks. Delvis skygge. Disse ikke-ideelle forhold fører til en uoverensstemmelse i solcelleanlæggets elektriske egenskaber, hvilket er bygget op fra få til tusindvis af solcelle paneler koblet i serie og parallelt for at nå et bestemt systemkrav. På grund af ubalance påvirkes hele PV-systemets ydeevne sammen med systemets levetid, som forringes på grund af spændingerne, der genereres grundet ubalancen i PV-systemet.

Dette Ph.D. studie er opdelt i to dele, for at analysere, diagnosticere og dæmpe virkningen af uoverensstemmelse i solcelleanlægget. I den første del undersøges krystallinsk silicium (c-Si) og tyndfilm solcellepanelteknologier for at analysere dem ved hjælp af infrarød termografi, temperaturmåling og spænding og effekt (PV) karakteristika under forskellige uoverensstemmelsesforhold. Derudover anvendes infrarøde termografiske billeder også til diagnoser af mismatcheffekten gennem en maskinindlæringsbaseret (ML) algoritme, dvs. Naive Bayes (nBayes) klassifikator. ML bruges til at detektere hotspots i c-Si PV-paneler. Den udviklede algoritme kategoriserer PV-panelets infrarøde billeder i tre forskellige kategorier, f.eks. normalt, defekt og hotspot. Metoden har en effektivitet på over 94%.

I anden del af afhandlingen, er teknikkerne, som er baseret på effektelektronik, blevet udviklet for at reducere virkningen af mismatch i et solcelleanlæg. De udviklede teknikker bruger smarte bypass-dioder og distribuerede elektroniske topologier, der fokuserer på differentieret effekt processing (DPP) for at reducere virkningen af mismatch. De udviklede topologier forbedrer udvindingen af energi fra systemet ved at reducere stress over komponenterne i topologien ved at minimere strøm svingninger, bedre spændingsudligning og forbedre ydelsen under alvorlige mismatch-forhold sammenlignet med allerede eksisterende løsninger. Derudover behandler DPP kun en lille effekt i stedet for at behandle hele effekten fra PV anlæg. Derfor er størrelsen på DPP-omformerne lille, og derfor kan let integreres i en PV-panelkoblingsboks. Desuden eliminerer DPP-konvertere problemet med multiple effekt punkter (MPP'er) i solcelle-PV-systemer, hvilket reducerer kompleksiteten i MPPT-algoritmer (maximum power point tracking). De foreslåede topologier analyseres gennem simulering og laboratorie eksperimenter. Derudover sammenlignes DPP-konverteren sammen med DC optimizer også med den nyeste løsning, dvs. bypass-diodeteknik under forskellige mismatch-scenarier for at analysere effektiviteten og ydeevnen af disse tre teknikker.

I forlængelse, undersøger Ph.D. undersøgelsen også integrationen af DPP-topologier på forskellige PV-streng-sammenkoblingsordninger, f.eks. serie-parallell (SP), total-

tværbundet (TCT), bro-bundet (BL) og central-tværbundet (CCT), for at analysere deres anvendelighed. Til dette formål overvejes et system med 4x4 PV-panel til analyse under forskellige uoverensstemmende forhold. Resultaterne viser, at DPP-omformerne kan integreres for SP- og CCT-forbindelser på grund af DPP-konverterstrukturen. Integrationen med SP og CCT viser imidlertid en forbedring af det samlede energiudbytte. Således kan integrationen af DPP med forskellige integrations muligheder være en lovende løsning til at forbedre ydelsen og effektiviteten af store solcelleanlæg.

# Acknowledgments

This Ph.D. thesis is a summary of the Ph.D. project ‘Mismatch effects and their mitigation techniques in the solar photovoltaic system’. This Ph.D. project is mainly supported by the Department of Energy Technology, Aalborg University, Denmark, Otto Mønstedts Fond, and Chief Minister Merit Scholarships (CMMS) / Ph.D. Foreign Scholarships, Pakistan. I would like to thank you for all the supports obtained from them.

First of all, I must start by thanking my sincere gratitude to my supervisors, Prof. Yongheng Yang and Assoc. Prof. Tamas Kerekes, for their patient and professional guidance throughout my Ph.D. project. This Ph.D. thesis could not be finalized without their support. I would also like to thank my co-supervisors, Assoc. Prof. Dezso Sera, for their consistent support, advice, and encouragement. I am honored to work with him. Special thanks to Prof. Sonia Leva, and Assoc. Prof. Alberto Dolara for their enthusiastic and continuous guidance during my study abroad at Politecnico di Milano, Milan, Italy.

I would also like to extend my heartfelt appreciation to Prof. Frede Blaabjerg who gave me the opportunity of this Ph.D. at Aalborg University. I would like to extend my gratefulness and thanks to all my colleagues and friends who helped me tremendously during my Ph.D. project. Many thanks to Dr. Hassan Abbas Khan, Dr. Mashood Nasir, Dr. Akif Zia Khan, Dr. Wenjie Liu, Dr. Zhongxu Wang, Muhammad Umair Mutarraf, Yiwei Pan, Jinkui He, and all my colleagues at the Department of Energy Technology, Aalborg University for their kind help.

I would like to express my sincere gratitude to my siblings, my wife, and my beautiful daughter Eliana Kamran for their endless love all the way. Without their support, this project would not be possible.

And the most important and special thanks to my parents Shah Wali Khan Niazi and Anwar Khatoon to whom I dedicate my Ph.D. work for their constant endless prayers, love, and support throughout my life.

Kamran Ali Khan Niazi

May 20, 2021

# TABLE OF CONTENTS

<b>Abstract .....</b>	<b>ii</b>
<b>Abstrakt.....</b>	<b>iv</b>
<b>Acknowledgments.....</b>	<b>vi</b>
<b>Report .....</b>	<b>1</b>
<b>Chapter 1.....</b>	<b>2</b>
1.1. Background .....	2
1.2. Project Motivation.....	11
1.3. Project Objective and Limitation .....	12
1.3.1. Research Question and Objectives .....	12
1.3.2. Project Limitations .....	12
1.4. Thesis Outline .....	13
1.5. List Of Publication .....	14
<b>Chapter 2.....</b>	<b>16</b>
2.1. Introduction.....	16
2.1.1. c-Si vs Thin-Film PV Panels Construction .....	16
2.1.2. Mismatch in c-Si and Thin-Film Solar PV Panels .....	18
2.1.3. Hotspots in c-Si and Thin-Film Solar PV Panel During Mismatch.....	19
2.2. Hotspots Detection and Classification by Using Machine Learning on Infrared (IR) Thermographic Images of c-Si Solar PV Panels .....	20
2.2.1. Hotspot Diagnostic and Classification Method .....	22
2.2.2. Experimental Results and Discussion .....	26
2.3. Summary and Conclusions.....	26
<b>Chapter 3.....</b>	<b>28</b>
3.1. Introduction.....	28
3.2. Smart Bypass Diode Solution .....	28
3.3. Differential Power Processing (DPP) Solutions .....	31
3.3.1. SCL-Based DPP Topology.....	31

3.3.2. Intrinsic-Capacitance-Based DPP Converter Topology for Solar PV Panels .....	35
3.4. Comparison between Bypass Diode, DC Optimizers, and DPP Converters .	39
3.5. Summary and Conclusions.....	42
<b>Chapter 4.....</b>	<b>46</b>
4.1. Introduction.....	46
4.2. Switched-Inductor-Based DPP Architecture in Parallel-Connected PV Strings .....	47
4.3. Switched-Capacitor-Based DPP Architecture in Parallel-Connected PV Strings .....	50
4.4. DPP Architecture in PV String Interconnection Schemes.....	51
4.5. Summary and Conclusions.....	56
<b>Chapter 5.....</b>	<b>58</b>
5.1. Thesis Contributions and Outcomes .....	58
5.2. Future Work .....	59
<b>BIBLIOGRAPHY .....</b>	<b>62</b>

# Report

# CHAPTER 1.

## 1. Introduction

This chapter presents the background and the motivation of the Ph.D. thesis, continues with research questions, objectives, and limitations encountered during the Ph.D. project. In the end, a list of the main contributions, which is achieved during the research work is presented along with a brief presentation of the thesis outline.

### 1.1. Background

Energy production from coal, natural gas, and other fossil fuels is limited and is not environmentally friendly. Therefore, it is necessary to replace them with environmentally friendly resources to reduce environmental pollution. Hence, energy production from wind and solar is increasing over the years with much popularity to address such issues, as depicted in Fig. 1.1. The energy generation from renewables is increased over the years up to 27.3% according to a report published by renewables in 2020 [1]. The report shows that solar energy is increased by an amount of around 115-GW and wind energy is increased by around 60-GW in 2019. Overall, the share of solar and wind energy until 2019 is about 2.8% and 5.9%, respectively. In recent years due to the decreasing cost of solar photovoltaic (PV) panels, solar PV energy has shown tremendous growth [2], [3]. The increasing trend of solar PV global capacity is shown in Fig. 1.2. Additionally, a recent report published by the International Energy Agency (IEA), the installed capacity of solar PV is more than 600-GWp [4], [5]. From the installed PV capacity, the contribution from crystalline-silicon (*c-Si*) solar PV technology is more than 90% due to high reliability and better long-term performance. There are also other PV technologies, e.g., thin-films

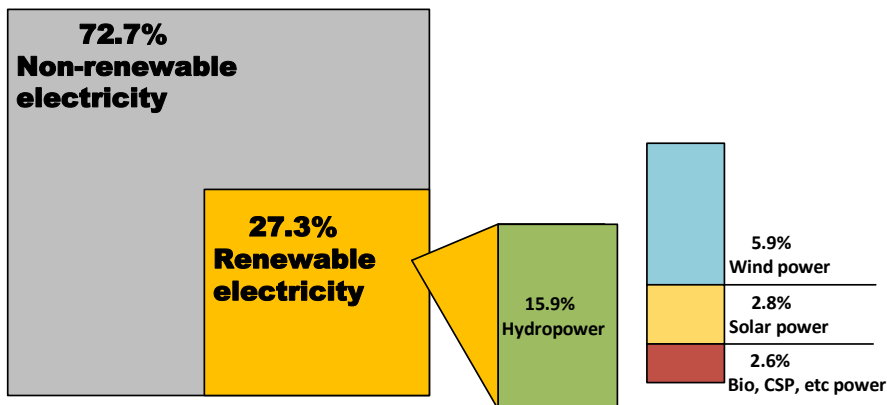
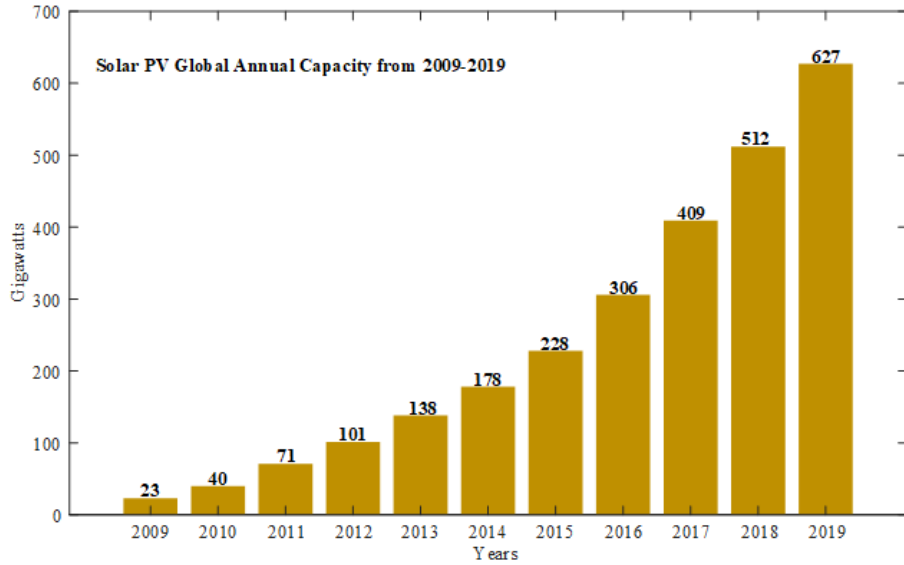
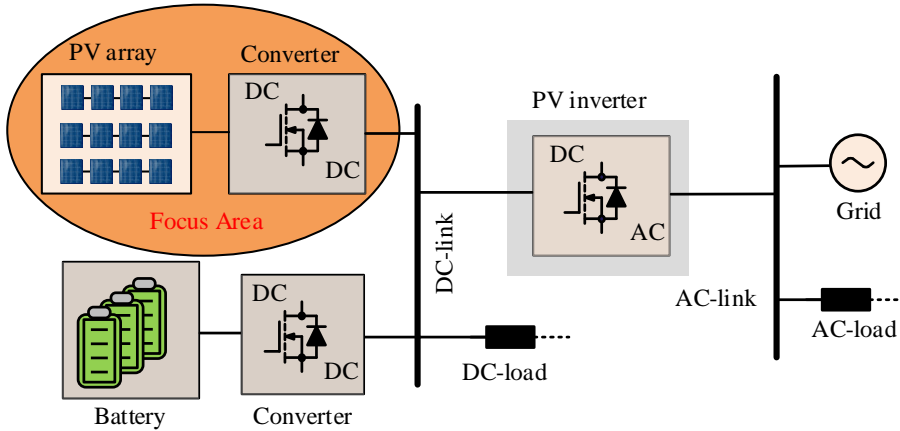


Fig. 1.1: Global estimated energy share of renewable sources from 2019 [1].



**Fig. 1.2:** Solar PV global capacity from 2009-2019 [1].

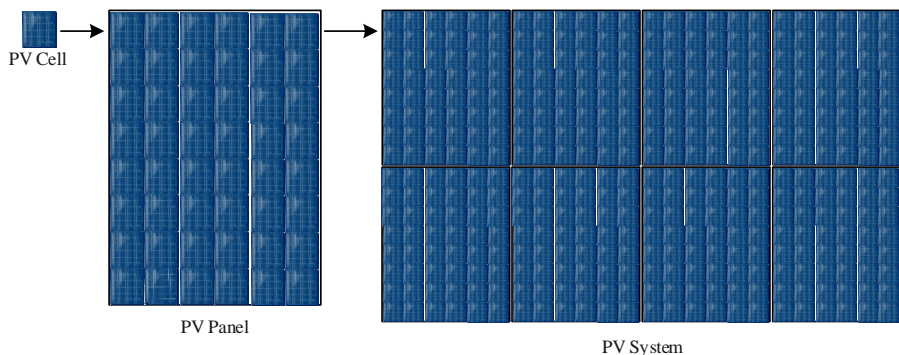


**Fig. 1.3:** A general schematic of the electrical system containing power generation sources, energy storage devices (batteries), DC-DC converters, DC-AC converters (inverters), and electrical load.

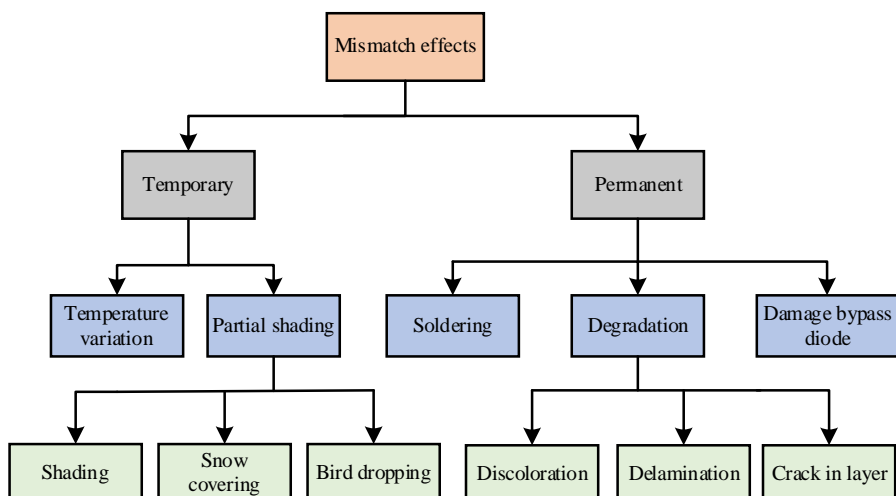
(amorphous-Si (*a-Si*), which are also installed but their performance and efficiency are lower when compare to c-Si [6]–[8].

An electrical system consists of various components, which are shown in Fig. 1.3, i.e., power generation sources, energy storage devices (batteries), DC-DC converters, DC-AC converters (inverters), and electrical load. These various electrical components are connected by a means of power electronic converters [9]. Therefore, highly





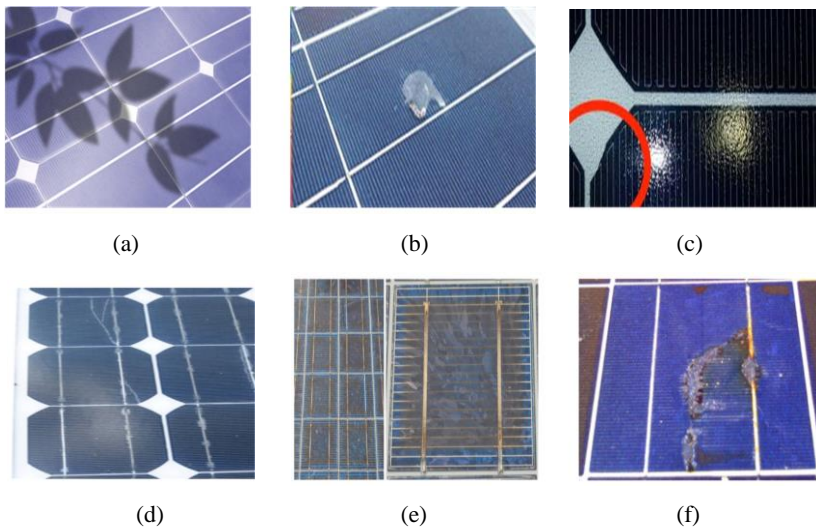
**Fig. 1.4:** A general schematic from a solar PV cell to a solar PV system.



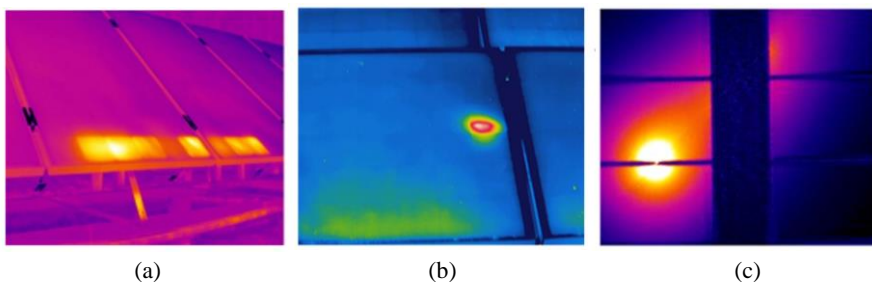
**Fig. 1.5:** Classification and possible causes of mismatch faults in solar PV panels.

efficient power electronic converters are required to transfer power from a source to consumers with a requirement of advanced control strategies.

A PV system consists of several solar panels and these panels are generally formed from a series combination of several solar cells, as shown in Fig. 1.4. The PV panels are connected in series/parallel or both series and parallel to achieve the required voltage and current level [10]. However, these connections make a PV system more sensitive to non-ideal environmental conditions. The difference of environmental conditions over the PV panels connected in the same system cause mismatch in the electrical characteristics of the system. This mismatch in the electrical characteristics of PV panels affects the performance and efficiency of the PV system [11]–[13].

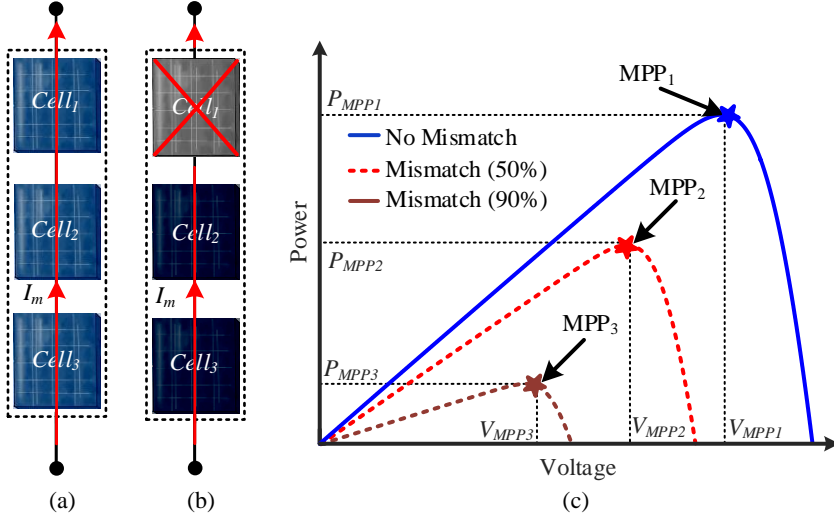


**Fig. 1.6:** Mismatched causes: (a) partial shading from leaves, (b) bird drop, (c) soldering, (d) cracks in PV panel, (e) discoloration, and (f) delamination due to burning [J4].



**Fig. 1.7:** Hotspot in solar PV panels: (a) partial shadow, (b) damage cells, and (c) damaged gridline [J4].

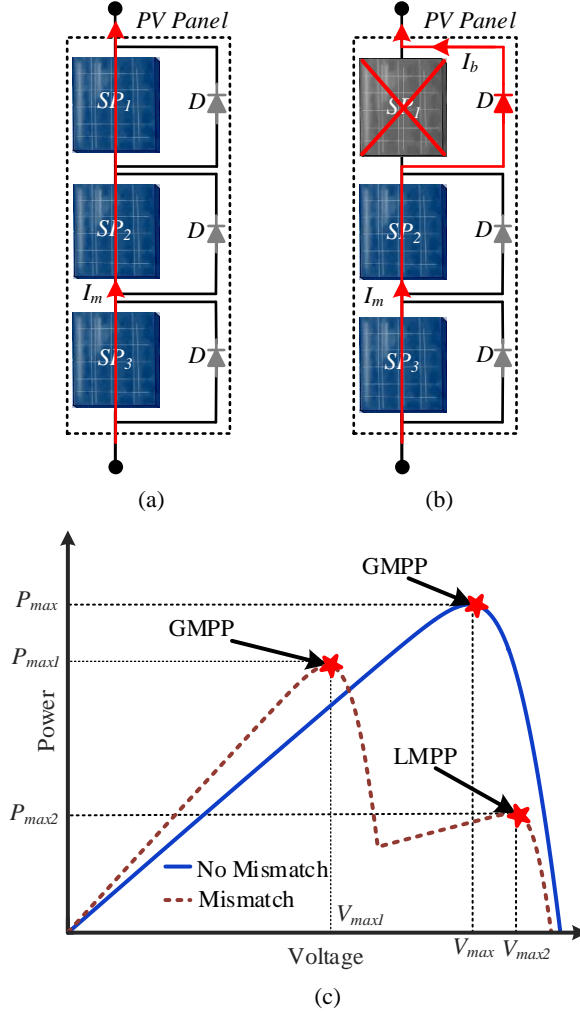
In continuation, the mismatch in PV can be classified into two categories, i.e., temporary and permanent mismatch faults, as shown in Fig. 1.5. For example, if the mismatch is caused by partial shading from trees and their leaves, bird drops, electric poles, and cloud shadow, etc., they are classified into temporary mismatch faults [J4]. Additionally, a mismatch caused by soiling and dust over the PV panels is also a type of temporary mismatch fault, which causes an energy reduction of the system up to 18.7% in a month [14], [15]. However, the mismatch caused by the internal cracks in PV cells, burning of PV cells, discoloration, and soldering errors, etc., are the causes of a permanent mismatch fault in the solar PV system [16]–[18]. Some of the temporary and permanent causes of mismatch faults are also shown in Fig. 1.6. Importantly, these mismatch faults introduce stresses over the whole PV panels or to some specific area of the PV panel by increasing the temperature of the affected panel area. These high-temperature areas of the PV panels are known as hotspots and some



**Fig. 1.8:** A series-connected photovoltaic (PV) cells: (a) a general schematic showing current flow under no shade, (b) a general schematic showing current flow when  $Cell_1$  is shaded, and (c) power-voltage ( $P$ - $V$ ) characteristics when  $Cell_1$  is not shaded and shaded 50% and 90%.

of the examples are shown in Fig. 1.7 [J4]. These hotspots affect the life of PV panels and may also cause permanent damage if it remains for a longer time [19]. Therefore, this Ph.D. aims to analyze the infrared (IR) thermal images of solar PV panels to diagnose the hotspots caused by mismatch to prevent them from permanent damage to the PV panels. Additionally, these IR images were also classified into various categories using machine learning so that defective panels can be separated from non-defective panels. Moreover, this can help to replace the defective panels with new panels to remove the mismatch in the system.

Normally, the PV panel consists of a series connection of 60-72 PV cells, as mentioned above [20]. For example, if any of the cell(s) is affected by partial shading or other non-ideal environmental situation then it also affects the other series-connected cells, which are operating under normal operating conditions, as depicted in Fig. 1.8 [21]. Hence, the overall power from a panel is affected and reduced, which are shown in the  $P$ - $V$  characteristic curves given in Fig. 1.8(c). Therefore, each PV panel consists of two or three series-connected PV sub-panels ( $SP_1$ ,  $SP_2$ , and  $SP_3$ ), which consist of a group of cells in each sub-panel, as shown in Fig. 1.9(a). In parallel to these sub-panels, there is a parallel-connected bypass diode  $D$  to limit the effect of mismatch [20]. The bypass diode  $D$  remained *OFF* under no mismatch, as depicted in Fig. 1.9(a). However, when there is a mismatch, the bypass diode associated with the affected PV sub-panel is turned *ON* and the current from the unaffected PV sub-panel starts to flow through this bypass diode  $D$ , as shown in Fig. 1.9(b). Hence, the bypass diode helped in maintaining the current coming from other series-connected



**Fig. 1.9:** A photovoltaic (PV) panels (*sub-panel*<sub>1</sub> ( $SP_1$ ), *sub-panel*<sub>2</sub> ( $SP_2$ ), and *sub-panel*<sub>3</sub> ( $SP_3$ )) with parallel-connected bypass diodes: (a) general schematic showing a current flow under no shading or mismatch, (b) current flow under mismatch when  $P_1$  is producing less than other two series-connected PV panels and is bypassed by a diode  $D$ , and (c) power-voltage ( $P$ - $V$ ) characteristics under shade and no-shade [C5].

unaffected PV sub-panels by bypassing the low power-producing PV sub-panel, as shown in Fig. 1.9(b). Now, the bypassed sub-panel has no contribution to the output power and the bypass diodes induce multiple power peaks (MPPs) in the power-voltage ( $P$ - $V$ ) characteristics of the system when they are in ON-state, as shown in Fig. 1.9(c). These MPPs increase the complexity of the multiple power point tracking (MPPT) algorithms to track the maximum peak from many other local peaks [22].

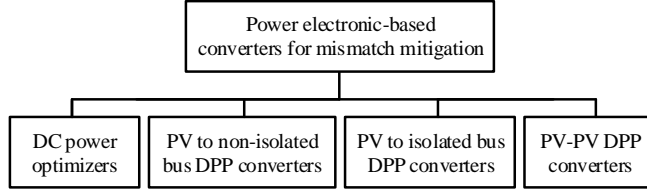
This maximum power peak is also known as a global maximum power peak (GMPP) and the algorithms that are used to track the global peak are known as global maximum power point tracking (GMPPT) algorithms [23]–[25].

To mitigate the effect of mismatch, there are power electronic-based solutions, which are more effective than simple bypass diode solutions [26]–[40]. The most commonly used power electronic solutions are mentioned in Fig. 1.10, i.e.,

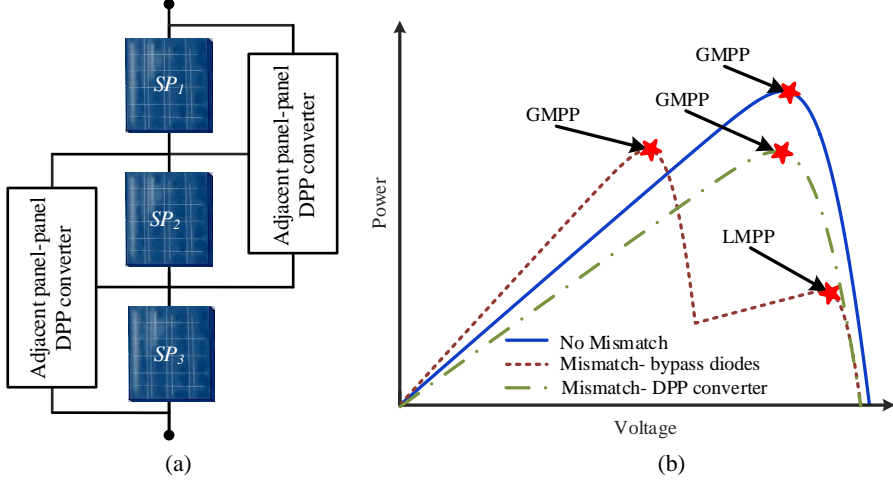
- DC power optimizers and
- Differential power processing (DPP) converters.

In **DC optimizers**, DC-DC converters (e.g., buck or boost) are used at the panel or sub-panel level [41], [42]. The converter processes the complete power from the PV panel or sub-panel level to mitigate the mismatch. The mismatch is mitigated by matching the current at the output of the DC-DC converters, which are connected in series with each other. In DC-optimizers the converters are processing the full power instead of just processing the small amount of mismatched power [43], [44]. Therefore, the selected components in DC-optimizers larger in size, higher in cost, and importantly lost more power than the DPP converters. In DPP converters, the converter is only processing the small portion of mismatched power instead of processing the whole power unlike DC-optimizers, which make them smaller in size and efficient than the other existed mismatch mitigation solutions [43], [45]–[55]. Therefore, DPP converters are becoming more effective and reliable solutions for power mismatch in solar PV applications [56].

Generally, **DPP converters** are categorized into three various categories [43], [57], which are mentioned in Fig. 1.10. The various DPP categories are **PV panel to the non-isolated bus** [58], **PV panel to an isolated bus** [36], [59], and **PV-to-PV DPP converters** [47], [49], [55]. In the PV panel to the non-isolated bus DPP converters, the secondary side of the converter is connected in parallel to the central inverter therefore, they share the same voltage. The secondary side or DC bus voltage of the DPP converter is high as it is the sum of the voltage of all available PV panels in the system. Therefore, the switches at the secondary side of the converters face high stress, which affects the performance and the life of the overall converter. In the second DPP topology, which is an isolated bus DPP topology, the secondary sides of this DC-DC DPP topology are in parallel. Additionally, the design complexity of the topology is high due to the independent selection of the DC bus voltage from the PV panel voltage. Moreover, the size and cost of isolated bus DPP topologies are higher due to more number of components along with a requirement of a transformer for isolation. The third category of DPP converter is PV to PV DPP converters. In PV to PV DPP converters, the converter allows the bi-directional flow of power and is non-isolated by nature. In PV to PV DPP converters, the power is processed and transferred through adjacent DPP converters. The general schematic diagram of the PV to PV DPP converter is shown in Fig. 1.11(a). It can be seen from Fig. 1.11(a), PV to PV

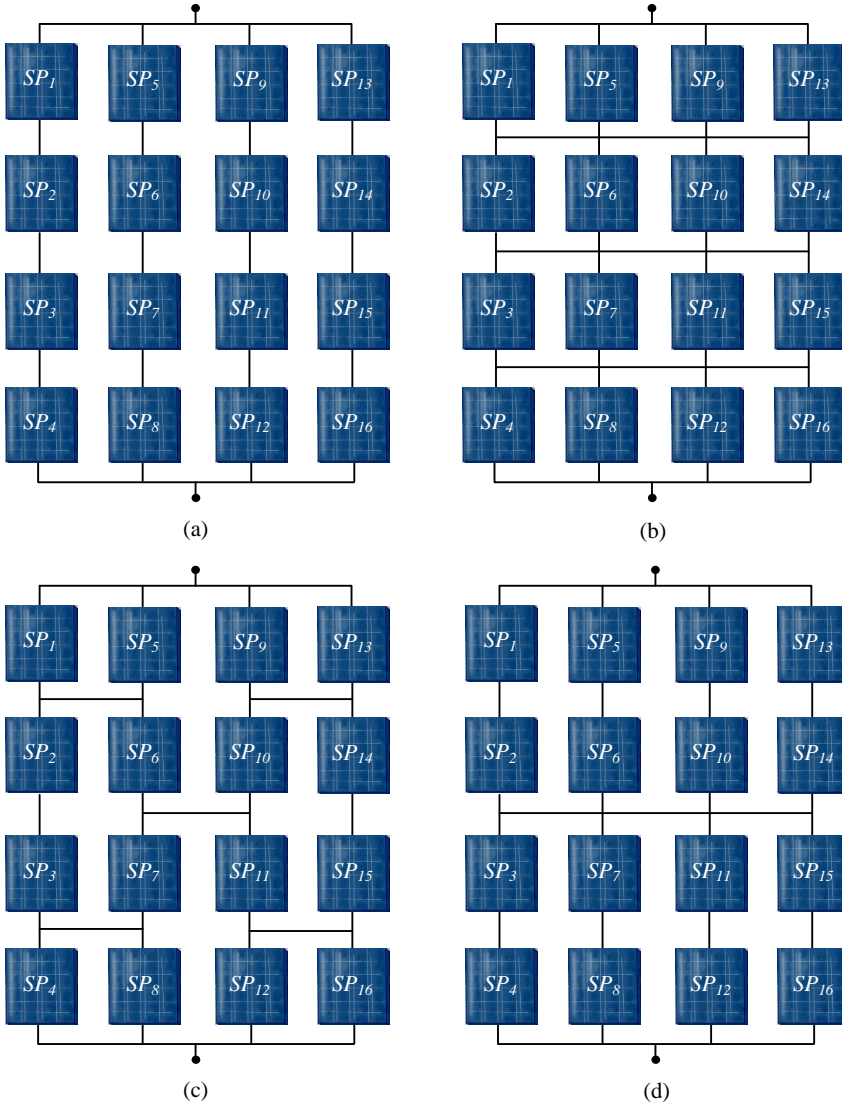


**Fig. 1.10:** Power electronic-based mismatch mitigation solutions [J5].



**Fig. 1.11:** Adjacent PV sub-panel to sub-panel level DPP converter [C5], [J5].

DPP converters consist of one less converter in comparison to the total number of PV panels. Moreover, it is designed according to the voltage of the PV panel instead of the main bus voltage, which reduces the stresses over the components available in the converter. Additionally, PV to PV DPP converters is simple, less complex, and cost-effective as compared to other DPP converter types. Several PV to PV DPP topologies existed in the literature, i.e., buck-boost, switched-capacitor (SC), resonant switched-capacitor (RSC), and energy recovery, etc. Overall, these DPP converters can be applied at the cell, sub-panel, or even at a panel level. However, they face various challenges, e.g., high losses during power processing, lack of extension flexibility, complex control structure, and low performance under severe mismatch conditions. Therefore, the PV-to-PV DPP class was selected during this Ph.D. study to improve the performance by proposing new DPP converters, which can perform better under severe mismatch conditions along with a simple control structure. Overall, the DPP converters process only the mismatched power and help in achieving voltage equalization across the PV panels. The voltage equalization eliminates the multiple power peak issues in the  $P$ - $V$  characteristic curves during mismatch, as depicted in Fig. 1.11(b). Hence, these DPP converters also decrease the complexity of MPPT algorithms to track the MPP of the system. Therefore, in this Ph.D. work, one of the focuses is the development of novel power electronic DC-DC converters based on



**Fig. 1.12:** Solar PV array interconnection schemes: (a) Series-Parallel (SP), (b) Total-Cross-Tied (TCT), (c) Bridge-Linked (BL), and Central-Cross-Tied (CCT) [J2].

DPP technology to extract maximum power from a solar PV system under a mismatch, e.g., partial shading.

In continuation, there are also PV string interconnection schemes to reduce mismatch effects caused by partial shading [60]–[63]. The most commonly used interconnection

schemes are series-parallel (SP) [64], total-cross-tied (TCT) [65], [66], bridge-linked (BL) [67], and central-cross-tied (CCT), which are shown in Fig. 1.12 for 4x4 PV array sub-panel system. From these interconnection schemes, the TCT is proved to be most effective during the non-ideal conditions, which also increases the life of the PV panels by 30%, as mentioned in the literature [62]. Additionally, the PV panels in these interconnection schemes are still equipped with parallel-connected bypass diodes to limit the mismatch effects. Furthermore, these interconnection schemes are divided into static and dynamic categories. In static interconnection schemes, the location of PV panels is fixed therefore, they are not able to change their arrangement. In dynamic configuration, the PV panels can change their positions by finding the best suitable arrangement where the effect of mismatch is minimum in the system [68]–[71]. The dynamic reconfiguration can be achieved by detecting the string current, short circuit current, panel voltage, panel irradiance, and temperature, etc. A dynamic reconfiguration, e.g., electronic array reconfiguration (EAR), uses the shading pattern to arrange the PV panels using electronic switches [64]. The control of the EAR is achieved by using the switching matrix. In continuation, there is another disperse interconnection scheme (SDS), which uses multiple PV panels in an array [68]. The SDS is very effective for PV array and yields higher energy but the control complexity and the cost of the system is very high. Hence, it is not feasible to use SDS [J2]. Overall, the dynamic reconfiguration uses relays and other similar switches, which require complex and time-consuming control algorithms to find the best suitable positions for the PV panels in the strings. Besides, the cost and complexity, the *P-V* characteristics of the overall interconnection scheme systems still compromise MPPs, which require GMPPT algorithms to track their global peak. Therefore, this Ph.D. study also works on the integration of the DPP converters with the above-mentioned various PV array interconnection schemes for the first time to analyze the performance and behavior of the overall system. For this purpose, the parallel-connected bypass diodes are replaced by the DPP converters in the various interconnection schemes shown in Fig. 1.12 to analyze their impact on the overall system performance under various mismatch conditions.

## 1.2. Project Motivation

As discussed above, there are several challenges in PV systems, which are needed to be addressed for the improvement of performance, reliability, and the energy yield of the overall system. Some of them are

- In-depth study of PV panel characterization under mismatch and their effect on different PV panel technologies.
- Analysis of infrared (IR) thermographic images of PV panels to study the different mismatch effects. For this purpose, image processing techniques and machine learning algorithms are needed to be explored.
- Improvement in the power electronic-based mismatch mitigation solutions focusing on differential power processing (DPP) converters.



- A comparison of DC optimizers, DPP converters with state-of-the-art solution, i.e., bypass diode method under various mismatch conditions.
- Analysis of power electronic-based DPP solutions at panel-level in different PV string inter-connection schemes, e.g., SP, TCT, and BL.

### **1.3. Project Objective and Limitation**

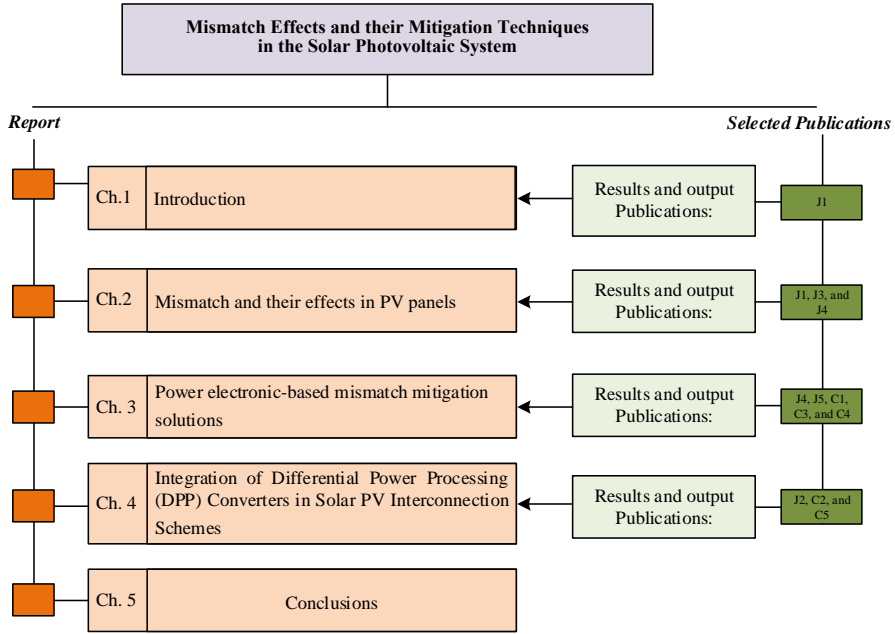
#### **1.3.1. Research Question and Objectives**

With the above-mentioned motivations, the final goal of this Ph.D. project is to enable an in-depth study of mismatch, and their effects on the solar PV system by considering different PV panel technologies along with exploring IR thermographic images. Moreover, the project also aims to explore new mismatch mitigation solutions in PV systems based on DPP converters and also check the possible connection of these DPP converters with various PV array inter-connection schemes. To do so, the following research questions are considered:

- i. What are the various effects of mismatch in different technology PV panels, e.g., crystalline-silicon (c-Si) and thin-film PV panels?
- ii. How image-processing and machine-learning can be used to develop a diagnostic methodology by using IR thermographic images?
- iii. What are the available power-electronic-based solutions for mismatch mitigation, selection of most suitable category from various power-electronic solutions (DPP converters and DC optimizers) by comparing them together and with state-of-the-art solutions, i.e., bypass diode method, and finally proposing a new simple power electronic-based solutions?
- iv. How to study and analyze the possibility of DPP converters in various PV string inter-connection schemes, e.g., SP, TCT, CCT, and BL?

#### **1.3.2. Project Limitations**

- Mismatch study is only considered for two PV technologies, i.e., crystalline-silicon (c-Si) and thin-film PV technologies. There are other technologies, e.g., bifacial, which are not covered in this work
- A diagnostic methodology using infrared thermographic images is only done for hotspots while there are other mismatch effects, e.g., cracks in cells, bus bar issues. These are not covered in this study.
- Power electronics-based mismatch detection algorithms are not included in this Ph.D. study.
- PV array connections, e.g., SP, TCT, CCT, and BL are only verified through simulations. No experimental validation is done.



**Fig. 1.13.** Thesis structure and related topics of each part.

## 1.4. Thesis Outline

The Ph.D. thesis is written as a collection of papers, therefore the thesis summary is followed by the publications related to the Ph.D. work done during the last 3 years. The document is structured in two main parts: Report and Selected Publications. The thesis structure is illustrated in Fig. 1.13, providing a guideline on how the content in the report is connected to the selected publications. In the report, a summary of research conducted during the Ph.D. study is presented, where the main results are based on the selected publications. The report is organized into five chapters. In Chapter 1, the introduction of the Ph.D. thesis is provided, where the background of the research topic and the objective of the Ph.D. study are discussed. Then, the following chapter deal with the study of mismatch effects in the PV system and their causes in different PV panel technologies. The main focus of Chapter 2 is to analyze the PV panels in detail how they look and behave under different mismatches. Therefore, infrared thermographic images are also used to analyze the panels and classify them into various categories using image processing and machine learning tools. In Chapter 3, the power electronics-based mismatch mitigation solutions are proposed, which improves the energy yield from a PV system under different non-ideal conditions. Furthermore, DPP converters and DC optimizers are also compared with state-of-the-art bypass diode solutions to analyze the effectiveness of these three solutions under various mismatch scenarios. For this purpose, the simulated system is also compared with a real PV system for the verification of achieved results. Then, in

Chapter 4, the commonly available DPP converters are applied to different PV array inter-connection schemes, e.g., SP, TCT, CCT, and BL, to study their applicability in these interconnection schemes for the first time. Finally, concluding remarks and the main contributions in this Ph.D. thesis are summarized in Chapter 5 and the future research perspectives are outline.

## 1.5. List Of Publication

The research outcomes during the Ph.D. study have been disseminated in several forms of publications: journal papers and conference publications, as listed in the following.

### Publications in Journals

- J1. S. Ahsan, **K. A. K. Niazi**, H. A. Khan, and Y. Yang, “Hotspots and performance evaluation of crystalline-silicon and thin-film photovoltaic modules,” *Microelectronics Reliability*, vol. 88–90, pp. 1014–1018, Sep. 2018.
- J2. **K. A. K. Niazi**, Y. Yang, M. Nasir, and D. Sera, “Evaluation of Interconnection Configuration Schemes for PV Modules with Switched-Inductor Converters under Partial Shading Conditions,” *Energies*, vol. 12, no. 14, p. 2802, Jan. 2019.
- J3. **K. A. K. Niazi**, W. Akhtar, H. A. Khan, Y. Yang, and S. Athar, “Hotspot diagnosis for solar photovoltaic modules using a Naive Bayes classifier,” *Solar Energy*, vol. 190, pp. 34–43, Sep. 2019.
- J4. **K. A. K. Niazi**, Y. Yang, and D. Sera, “Review of mismatch mitigation techniques for PV modules,” *IET Renewable Power Generation*, vol. 13, no. 12, pp. 2035–2050, Jun. 2019.
- J5. **K. A. K. Niazi**, Y. Yang, T. Kerekes, and D. Sera, “Simple Mismatch Mitigating Partial Power Processing Converter for Solar PV Modules,” *Energies*, vol. 14, no. 8, p. 2308, Apr. 2021.

### Publications in Conferences

- C1. **K. A. K. Niazi**, Y. Yang, H. A. Khan, and D. Sera, “Performance Benchmark of Bypassing Techniques for Photovoltaic Modules,” in 2019 *Proc. IEEE Applied Power Electronics Conference and Exposition (APEC 2019)*, pp. 3164–3168 Mar. 2019.
- C2. **K. A. K. Niazi**, Y. Yang, W. Liu, and D. Sera, “Sub-Module Level Differential Power Processing for Parallel-Connected Architecture in Photovoltaic Systems,”

in *Proc. 2019 21st European Conference on Power Electronics and Applications (EPE '19 ECCE Europe)* pp .1-9, Sep. 2019.

- C3. **K. A. Khan Niazi**, Y. Yang, J. He, A. Z. Khan, and D. Sera, “Switched-Capacitor-Inductor-based Differential Power Converter for Solar PV Modules,” in *Proc. 2019 IEEE Energy Conversion Congress and Exposition (ECCE 2019)*, pp. 4613–4618, Sep. 2019.
- C4. **K. A. K. Niazi**, Y. Yang, and D. Sera, “Intrinsic-Capacitance-based Differential Power Processing for Photovoltaic Modules,” in *Proc. 2020 22th Workshop on Control and Modeling for Power Electronics (COMPEL 2020)*, pp. 1–6, Nov. 2020.
- C5. **K. A. K. Niazi**, Y. Yang, and D. Sera, “Architecture for Parallel PV Strings using the Switched-Capacitor-Based Differential Power Processing Technique,” in *Proc. 2020 The 10th IET International Conference on Power Electronics, Machines and Drives (PEMD 2020)*, in press, Dec. 2020.

# CHAPTER 2.

## 2. Mismatch Effects on Solar PV Panel Technologies

This chapter presents in detail information about the mismatch causes and their effects in the solar PV system containing two commonly used solar panel technologies. The considered panel technologies were crystalline-silicon (c-Si) and thin-film, which were also considered to analyze the mismatch effect using infrared (IR) thermography. Additionally, this chapter also discusses the detection and classification of hotspots in solar PV panels using machine-learning (ML) on IR thermographic images of c-Si solar panels.

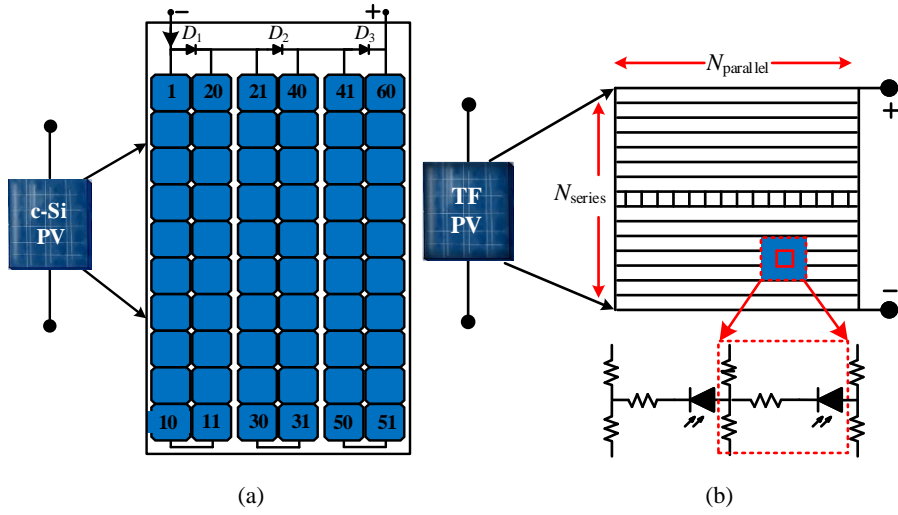
### 2.1. Introduction

To understand the impact of mismatch on two commonly used PV panel technologies, i.e., crystalline-silicon (c-Si) and thin-film, various experimental details are presented in J1 and J4 publications. In these publications, the behavior of these panel technologies is analyzed in detail by setting up various mismatch cases. These panels are studied through the analysis of power-voltage ( $P$ - $V$ ) characteristic curves, the thermal images, and the temperature across the infield installed PV panels under various partial shading conditions. These findings are described in the coming sections.

In continuation, the reliability of PV panels is highly affected by mismatch effects. The most common mismatch effect is the hotspot effect. Therefore, in publications J1 and J3, the hotspot occurrence in c-Si PV panels is studied in detail. Moreover, in J3, a hotspot detection and classification method is proposed. The hotspots under various mismatch scenarios are detected and classified by using a Naive Bayes (nBayes) machine learning (ML) classifier on solar PV IR thermal images. These IR thermal images are classified into three various categories, namely: (i) defective with hotspot, (ii) non-defective with hotspot (NDH), and (iii) non-defective without hotspots (NDNH). The proposed diagnostic methodology is shortly described next and a more detailed exploration of the method is presented in publication J3.

#### 2.1.1. c-Si vs Thin-Film PV Panels Construction

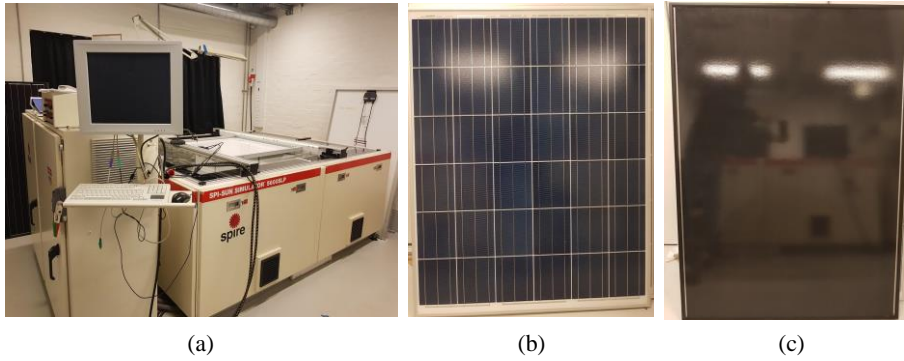
To understand the impact of mismatch in c-Si and thin-film panels, it was important to understand the construction of these PV panels. As the construction of both panel technologies is different, hence, the impact of mismatch is different. Therefore, J1 explains the construction of these two PV panel technologies, and their constructions are also shown in Fig. 2.1.



**Figure 2.1:** Internal structure of solar PV panel: (a) crystalline-silicon (c-Si) and (b) thin-film.

The c-Si PV panels are the mature technology, which is shown in Fig. 2.1(a). These are the most commonly and frequently used PV panels, which consist of 60-72 series-connected cells [20]. In c-Si technology, the PV cells contribute individually to the output power and the overall output voltage is also the sum of the individual voltages of the series-connected PV cells, which are acting as an individual DC voltage source [72]. However, the currents of c-Si PV cells must be the same due to their series-connection otherwise, it will create a mismatch. Therefore, bypass diodes ( $D_1$ ,  $D_2$ , and  $D_3$ ) are connected in parallel across the group of 20-24 series-connected PV cells, which are named as PV sub-panels, as shown in Fig. 2.1(a). These diodes are used to reduce the effect of mismatch between series-connected PV cells because the current supplied by a shaded PV cell is lower than the non-shaded PV cell [C2]. Hence, a mismatch is created due to a current difference and a cell with a low producing current starts to act in the reversed bias mode. Therefore, it is important to use a bypass diode to prevent the PV cell to reach its reverse breakdown voltage and to avoid the effect of shaded cells on the other series-connected non-shaded sub-panels. Additionally, the reverse-biasing of cells causes power dissipation, which affects the life of the PV cell and in turn whole panel. Furthermore, the effect of mismatch in c-Si becomes more worst with an increase of PV cell size because the current of a PV cell increases with its size. More details are presented in a publication J1.

In continuation, the internal structure of the thin-film PV panels is shown in Fig. 2.1(b). A thin-film PV panel consists of series-connection of PV cells, which are long, narrow, and rectangular in shape [73]. In thin-film panels, there is an intrinsic semiconductor layer between the p- and n-region, which creates high tolerance, which is normally enough to overcome the effect of reverse voltage during the mismatch in

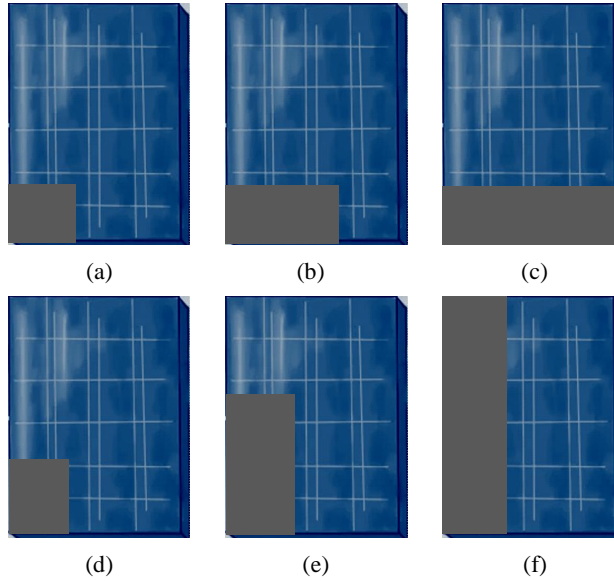


**Figure 2.2:** Experimental test setup: (a) SPI-SUN 5600 SLP apparatus used for experiments, (b) c-Si solar PV panel, and (c) thin-film (TF) PV panel.

one PV panel [J1]. Additionally, in a thin-film PV panel, a PV cell consists of sub-cells, which are parallel in connection. Hence, it becomes the major reason for the reduction of mismatch effect. Overall, the unique 2-D geometrical structure of thin-film panels allows the reduction of mismatch, which also reduces the possibility of the occurrence in high reverse bias voltages [J1]. Additionally, the thin-film PV panels consist of only one parallel-connected bypass diode per panel instead of many diodes like c-Si. Their electrical model and other details are presented in J1 publications.

### 2.1.2. Mismatch in c-Si and Thin-Film Solar PV Panels

To analyze and compare the effect of mismatch in c-Si and thin-film solar PV panels, experiments were performed by using SPI-SUN5600 test-rig, which is shown in Fig. 2.2(a). This test setup was used to extract the  $P$ - $V$  characteristics curve of these panels under various mismatch scenarios. For the tests, 150-W c-Si and thin-film PV panels were considered, which are also shown in Figs. 2.2(b) and (c). The c-Si solar PV panel in Fig. 2.2(b) consists of three bypass diodes and a thin-film consists of one bypass diode in Fig. 2.2(c). Moreover, the mismatch scenarios were developed for the analysis, which is also given in Fig. 2.3. In these mismatch scenarios, the PV panels were covered horizontally and vertically in three steps, as shown in Fig. 2.3. These mismatch scenarios were used to acquire the  $P$ - $V$  characteristic curves that helped in understanding and analyzing the working principle of these panel technologies, as shown in Fig. 2.4. In Figs. 2.4(a) and (b), horizontal shading (HS) and vertical shading (VS) are shown over the c-Si panel. It can be seen from Fig. 2.4(a) that during HS, the power output decreases with an increase of shading because each PV cell is the source of current along with providing the path for the current coming from other PV cells in series. Therefore, the increase of HS blocks the flow of current, which becomes the reason for the power lost as the path for the current is blocked when c-Si is completely shaded from the bottom. However, the VS in c-Si, which is shown in Fig. 2.4(b), only one sub-panel is shaded while the other two PV sub-panels are not shaded. Therefore,



**Figure 2.3:** Mismatch scenarios with horizontal shading (HS) and vertical shading (VS): (a) 33% HS, (b) 66% HS, (c) 100% HS, (d) 33% VS, (e) 66% VS, and (f) 100% VS.

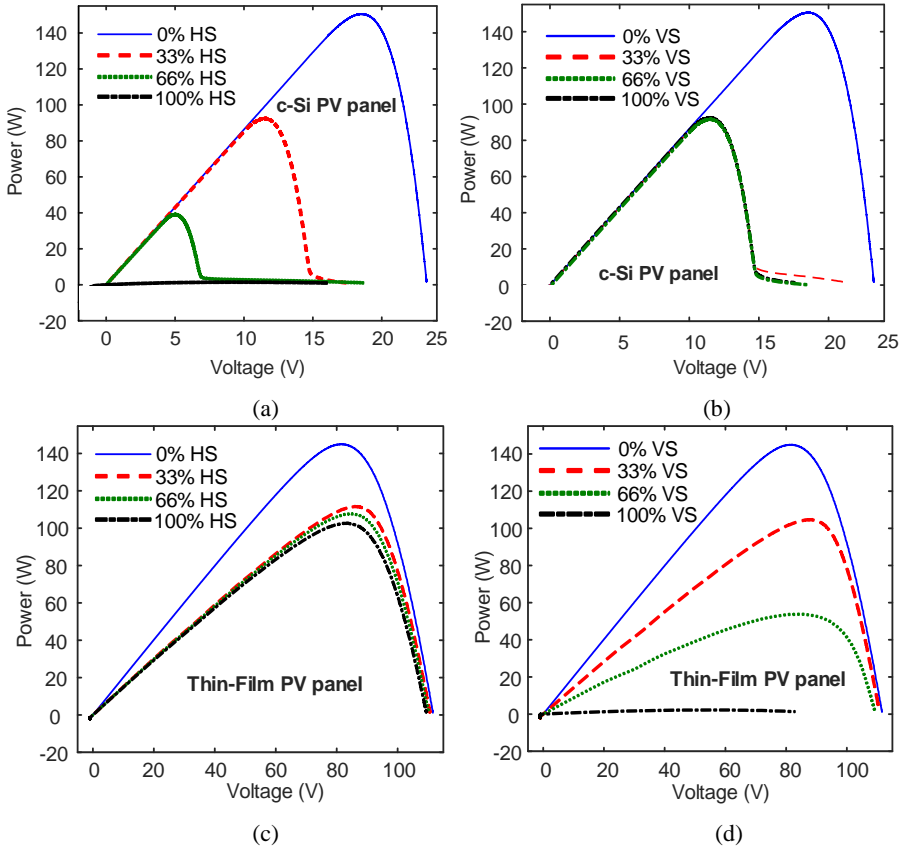
two-third of the power is still available at the output while the shaded sub-panel is bypassed by the bypass diode.

In continuation, the effect of HS and VS in thin-film is shown in Figs. 2.4(c) and (d). It can be seen from these figures, the effect of shading is different from the c-Si PV panel and it is because of the different internal structure of thin-film, as discussed above. In thin-film PV, the HS affects a small part of the PV power. However, the VS completely blocks the current flowing through the long and narrow vertical PV cells in a thin-film panel. Therefore, the output power is completely zero for a mismatch scenario shown in Fig. 2.3(f). More details and results are presented in Publication J1.

### 2.1.3. Hotspots in c-Si and Thin-Film Solar PV Panel During Mismatch

Mismatch in solar PV panels can also cause hotspots because the shaded part of the PV panel dissipates power as discussed before. Therefore, the high-temperature part of the PV panel appears as red and hotter than the other part of the same PV panel, as depicted above in the thermal images shown in Fig. 1.7. In continuation, these hotspots can affect the performance and the life of semi-conductor solar PV panels. Additionally, these hotspots can be categorized into temporary as well as permanent depend on their cause. For example, if the mismatch is caused by passing clouds and bird drops, then it can be labeled as a temporary hotspot. Otherwise, if the mismatch



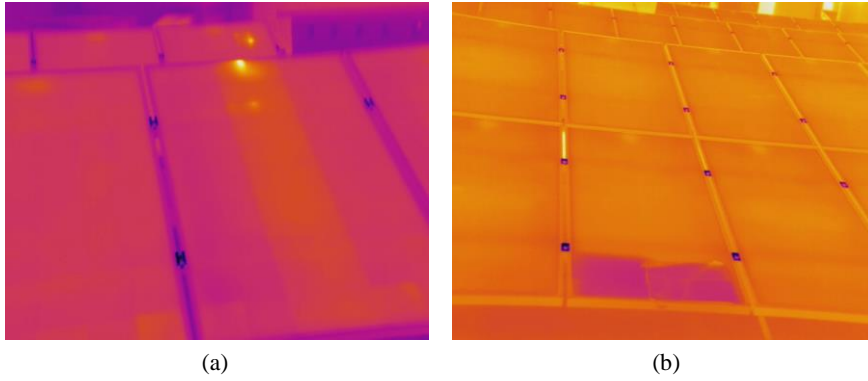


**Figure 2.4:** Power-voltage (P-V) curve under mismatch scenarios: (a) HS on c-Si, (b) VS on c-Si, (c) HS on thin-film, and (d) VS on thin-film.

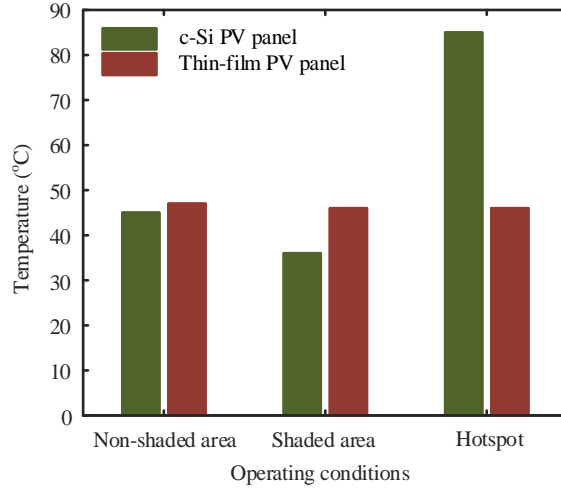
is caused by a damaged cell or some permanent shading from the chimney then it can be labeled as a permanent hotspot. Therefore, to study the behavior of mismatch in c-Si and thin-film PV panels, the analysis of hotspots was important. The thermal images are shown in Fig. 2.5 where Fig. 2.5(a) is for the c-Si and Fig. 2.5(b) is for the thin-film PV panel under mismatch. Additionally, the temperature of these PV panels was also measured at the shaded and non-shading areas by using a temperature gun, which is given in Fig. 2.6. More detailed explanations and results are presented in the publications J1 and J4.

## 2.2. Hotspots Detection and Classification by Using Machine Learning on Infrared (IR) Thermographic Images of c-Si Solar PV Panels

Infrared (IR) thermographic images of solar PV panels are commonly used to find visual identification of defects and other degradations, which are not easily detectable

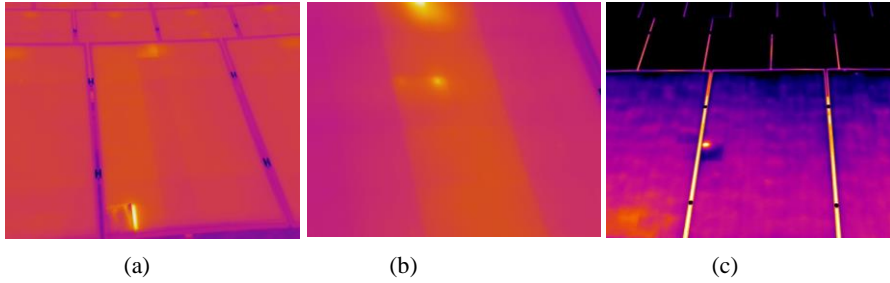


**Figure 2.5:** Thermal image of c-Si and thin-film PV modules: (a) mismatch in c-Si panel due to damage cell, and (b) thin-film PV panel under mismatch due to the bottom part of the shaded panel.




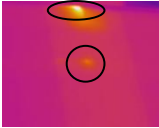


**Figure 2.6:** Effect of shading in terms of temperature on c-Si and thin-film PV modules under various conditions.

using the human eye, as shown in Fig. 2.7. However, it is difficult for a larger PV plant, which consists of thousands of PV panels to analyze each panel one by one to find defects. Therefore, in this regard, we have developed a non-invasive machine learning-based diagnostic method, which diagnoses and classifies the solar PV panel IR thermal images into various three categories, i.e., (1) Defective, (2) Non-defective with hotspots (NDH), and (3) Non-defective without hotspots (NDNH), as shown in Fig. 2.7 and Table 2.1 [J3].



**Figure 2.7:** Hotspots in solar PV panels: (a) shadow, (b) damage cells, and (c) damage cells.

**Table 2.1:** Thermal images and tempature of specific areas.

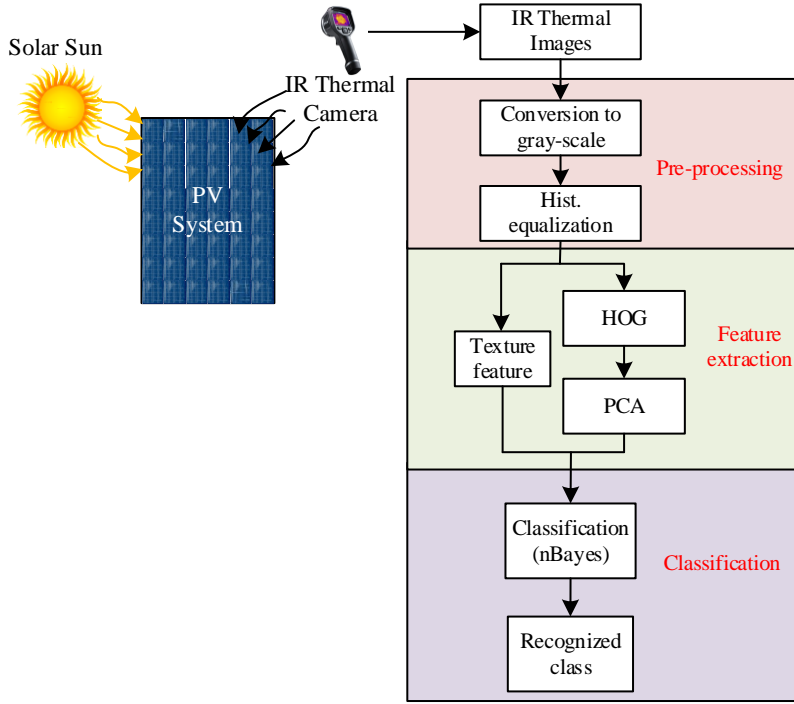
IR Thermal images				
Cause, Temperature	No shading, 60 °C	Damage, 77 °C	Shaded, 73 °C	Bird drop, 69 °C

This method can be used by the PV plant operators to identify the solar panels in the large as well as in the small systems to find the panels, which are creating a mismatch. Furthermore, if the mismatch is created by a temporary cause as discussed above, e.g., dust, birds drop, then it can be clean by the service provider. However, if the cause is permanent then the specific panel can be replaced timely before it starts to affect the other panel in the system.

In the next sections, this chapter will present the main concepts and steps used for the diagnostics and classification of PV panel thermal images. The concept was validated on a 42.24-kW system, which was analyzed and tested using a FLIR-Pro 640 thermal camera. More details regarding the system are presented in a publication J3, whereas the main flow diagram and results are also presented in the next coming sections.

### 2.2.1. Hotspot Diagnostic and Classification Method

The block diagram of the methodology containing the identification and classification of PV panel IR thermographic images using the nBayes-based classification method is given in Fig. 2.8. The whole process consists of various steps and each step has its importance for the achievement of the desired result. These steps are (i) data acquisition, (ii) pre-processing of the acquired data, (iii) feature extraction from the pre-processed data, (iv) training of model using the extracted features, and (v) classification.



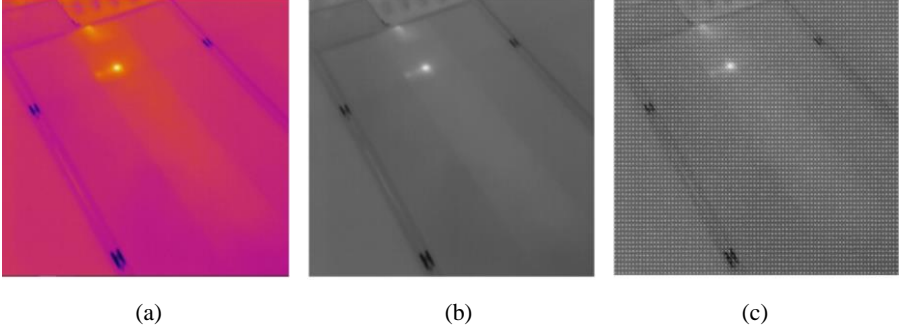
**Figure 2.8:** Machine-learning-based hotspot diagnostic and classification method.

**i. Data acquisition**

The data was acquired using a FLIR thermal camera, which has captured the images with a resolution of 640x512 with a bit depth per pixel per color channel of 8 [J3]. The acquired data set was categorized into the three various categories, as mentioned above for creating ground truth data. Overall, there were 375 images from which 130 were defective class, 125 from NDH class, and 120 from NDNH class.

**ii. Pre-processing**

Before training and classification, it was important to pre-process the acquired data. The pre-processing increased the textural information of the thermal images. Additionally, pre-processing also increased the reliability of the data. During pre-processing of the RGB image of a defective panel is shown in Fig. 2.9(a). Firstly, the RGB image was converted into a gray-scale [J3]. Afterward, histogram equalization was used to increase the contrast of the gray-scale image, as shown in Fig. 2.9(b). The image after histogram equalization is shown in Fig. 2.9(c).



**Figure 2.9:** Conversion of solar panel thermal image of a defective panel: (a) RGB image, (b) gray-scale image, and (c) HOG image [J3].

### iii. Feature extraction (Texture features and HOG features+PCA)

After pre-processing, texture and histogram of gradient (HOG) features were extracted from the pre-processed images to improve the process of identification and classification. In total, 182 features were extracted where 52 were texture and 130 were HOG features. The extracted texture features from the pre-processed image were contrast, energy, homogeneity, and correlation. Moreover, these texture features were calculated at four different values of the inter-sample spacing pixels with a distance equal to 1, 2, 3, and 4 at four uniformly distributed angular directions, i.e.,  $0^\circ$ ,  $45^\circ$ ,  $90^\circ$ , and  $135^\circ$ , as shown in the boxplot given in Fig. 10. Additionally, the visualization of the texture features map was done by a sliding window of size  $3 \times 3$  through equations (2.1)-(2.4)

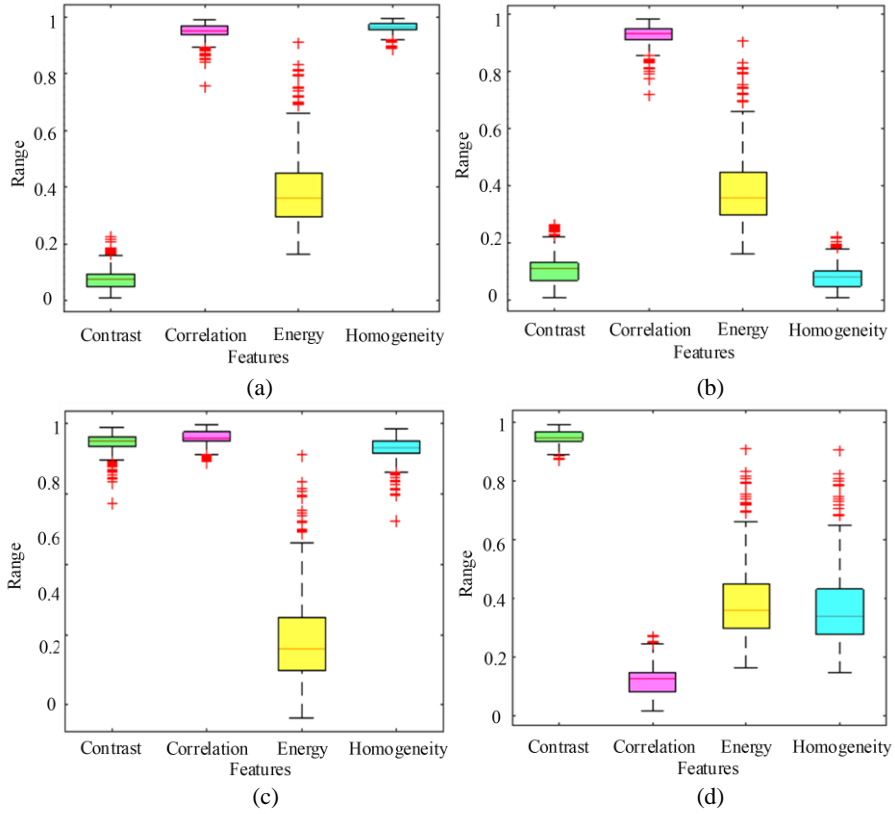
$$Contrast = \sum_{i,j=0}^{N-1} (i-j)^2 \times m_{ij} \quad (2.1)$$

$$Energy = \left( \sum_{i,j=0}^{N-1} m_{ij}^2 \right)^{\frac{1}{2}} \quad (2.2)$$

$$Homogeneity = \sum_{i,j=0}^{N-1} \frac{m_{ij}}{1 + |i-j|^2} \quad (2.3)$$

$$Correlation = \sum_{i,j=0}^{N-1} \frac{(i-\mu) \times (j-\mu) \times m_{ij}}{1 + \sigma^2} \quad (2.4)$$

where  $i$  and  $j$  represent the location of the pixel in the image,  $m_{ij}$  is the pixel value,  $N$  indicates the number of gray levels in the image,  $\mu$  is the mean, and the variance of the pixel is denoted by  $\sigma^2$  [J3].

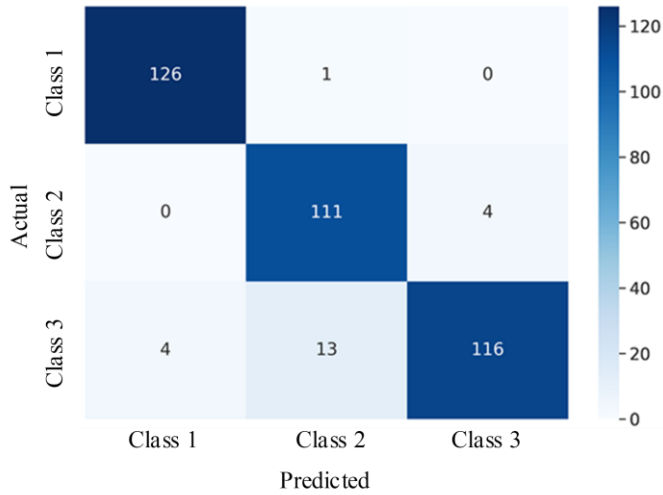


**Figure 2.10:** Boxplot showing different texture features at various angles: (a)  $0^\circ$ , (b)  $45^\circ$ , (c)  $90^\circ$ , and (d)  $135^\circ$ .

In continuation, the HOG features were obtained using a window or filter of  $4 \times 4$  on an image size of  $640 \times 512$ . Afterward, the texture and HOG features were concatenated but before that, a principal component analysis (PCA) was applied to the HOG features to remove the redundant information from these extracted features. Additionally, PCA also helped to reduce the dimensions of the data, which helped in making the process more efficient with improved accuracy and decreased computational time. The whole methodology is described in Publication J3.

#### iv. Training

After extracting the texture and HOG feature, a k-fold leave-one-out cross-validation method was used to train the dataset containing the thermal images [J3]. In this method,  $k-1$  thermal images were used to train the classifier and the remaining image was used for the testing of the trained classifier. More details of the training method are given in Publication J3.



**Figure 2.11:** Confusion matrix of proposed model.

**v. Classifier selection**

Finally, after training, a nBayes classifier was used, which calculates the probabilities for the input thermal images, and based on the obtained probability it classifies the input image into one of the defined three categories.

## 2.2.2. Experimental Results and Discussion

The performance of the proposed algorithm was insured from the confusion matrix, which is given in Fig 2.11. The diagonal values in the confusion matrix show the correct classification of the testing images. In Fig. 11, 353 images were classified correctly from 375 images. Hence, the efficiency of 94.10% was achieved using the nBayes classifier. More details of the whole method are described in Publication J3.

## 2.3. Summary and Conclusions

This chapter discusses the two commonly used types of PV panels (c-Si and thin-film) along with their internal construction to make a comparison between them. For comparison, experiments were performed using SPI-SUN 5600 SLP apparatus under various mismatch cases for the analysis of the electrical characteristics of these panels. Additionally, thermographic IR images of two individual PV systems contain c-Si and thin-film panels were also analyzed. Moreover, temperatures of various panels with and without mismatch in these two systems were also measured using a temperature gun. All these data were used to analyze and compare the effect of mismatch between these two-panel technologies. Overall, the analysis shows that the effect of mismatch in thin-film PV panels is lower than that of c-Si panels.

In the last part of this chapter, a machine-learning (ML)-based diagnostic method was developed and tested on c-Si solar panel thermal images. This method was used to detect and classify the solar thermal images into three categories, i.e., NDH, NDNH, and defective. For classification, nBayes ML technique was used by using the texture (i.e., contrast, correlation, energy, and homogeneity) and HOG features. Overall, the proposed classification method has achieved an efficiency of 94.10%.



# CHAPTER 3.

## 3. Power Electronic-Based Mismatch Mitigation Solutions

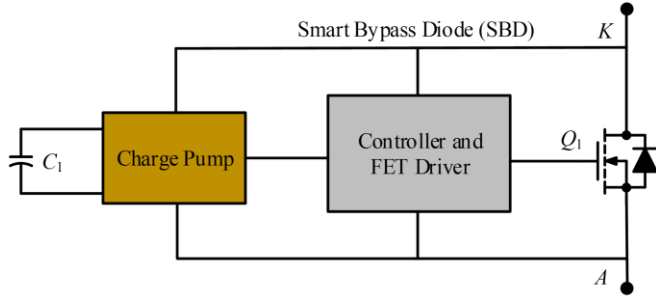
Many research efforts have been made to improve the performance of solar PV systems under partial shading and other mismatch conditions by presenting various power-electronic-based topologies. Considering the complexity, performance, and size, these topologies can be improved. Therefore, this section presents different power-electronic-based simple solutions that helped in the reduction and mitigation of mismatch effects in solar PV systems. Additionally, various case studies are also conducted that helped in the validation of the work. Moreover, this chapter also presents a comparison study of three important solutions that helped in the performance improvement of PV systems, i.e., bypass diode, DC optimizers, DPP converters. The pros and cons of these three solutions are discussed in this chapter by considering various real-time scenarios.

### 3.1. Introduction

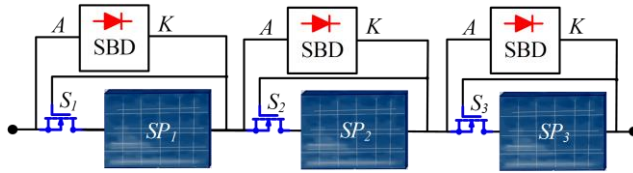
To select the proper mismatch mitigation topology, the required application, and other requirements related to size, cost, complexity, and control methodology was considered. As discussed in previous chapters, the bypass diode topology is not suitable to reduce the effect of mismatch where the non-ideal conditions are frequent. Therefore, in this chapter, various topologies are explored, which are smart bypass diode with series MOSFET, switched-capacitor-inductor (*SCL*)-based DPP topology, and intrinsic-capacitance-based DPP converter topology. These proposed topologies are presented in various publications, i.e., C1, C3, C5, and J5, respectively. Additionally, a summary of different mismatch mitigation techniques is also reported in the publications J4 and J6. These publications proposed a comparison among different topologies through various electrical parameters along with presenting the main advantages, disadvantages, and appropriate applications for specific topologies by considering their practical implementation.

### 3.2. Smart Bypass Diode Solution

In this section, a topology is discussed that can be used to reduce the effect of mismatch. This topology was presented in a publication C1. In this topology, a smart bypass diode (*SBD*) shown in Fig. 3.1 was used along with a MOSFET ( $S_1$ ,  $S_2$ , or  $S_3$ ), which was connected in series with a solar PV sub-panel ( $SP_1$ ,  $SP_2$ , and  $SP_3$ ), as shown in Fig. 3.2. The result achieved from this topology showed an improvement in the performance of the overall system by reducing the bypass diode losses along with the reduction of reverse voltages across the shaded cells. The lower bypass diode losses



**Figure 3.1:** Internal structure of smart bypass diode.



**Figure 3.2:** A parallel-connected smart bypass diodes (SBD) with a series MOSFET.

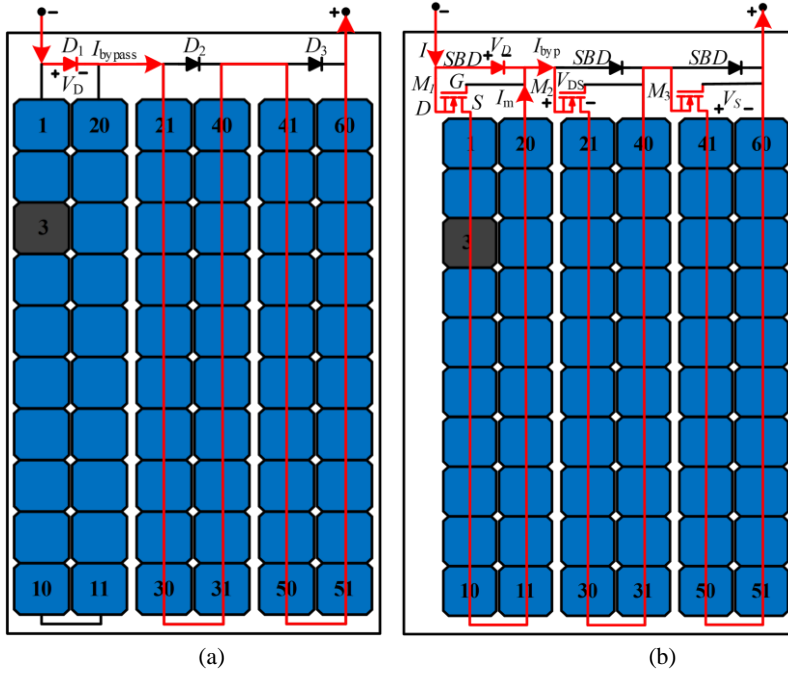
were due to the lower  $ON$ -state resistance of SBD. Additionally, the reduction of reverse voltage across the shaded cells was due to the on-state resistance of MOSFET ( $R_{on}$ ), which shared the reverse voltage of the shaded cells. This sharing of the reverse voltage between the shaded cells and  $R_{on}$  decreases the temperature of the shaded PV cells. Hence, that causes the reduction of stresses over these cells. Hence, it improves the overall reliability of the cell as well as the PV panel.

As mentioned above, the methodology shown in Fig. 3.2 helped in the sharing of reverse voltage across the shaded cell through  $R_{on}$  of the series MOSFET ( $S_1$ ,  $S_2$ , and  $S_3$ ). Additionally, the Gate to Source ( $V_{GS}$ ) voltage of series MOSFET is equal to the respective sub-panel voltage by which it is connected in series. Therefore, there is no need for a control circuit or external supply to turn this MOSFET  $ON$  as the MOSFET is turned  $ON$  automatically by the panel voltage. The voltage across the shaded cell ( $V_{shdcell}$ ) can be obtained as

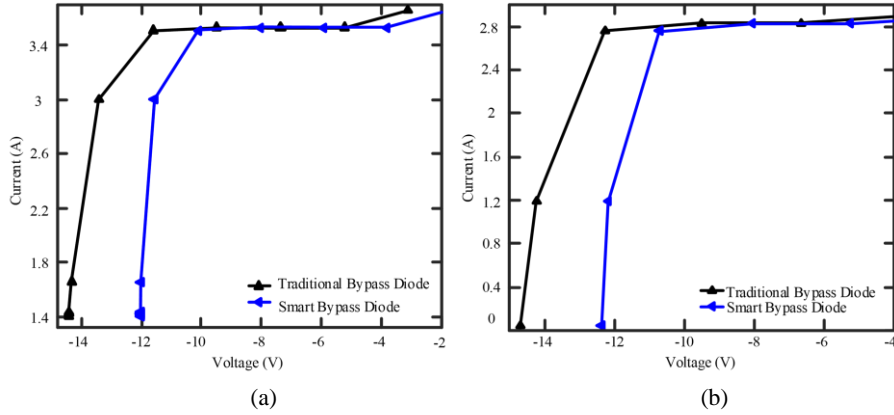
$$V_{shdcell} = (N-1)V_{cell} + V_D - V_{DS} \quad (3.1)$$

where  $N$  is the number of  $PV$  cells in a sub-panel,  $V_{cell}$  is the voltage of a  $PV$  cell,  $V_D$  is the voltage of a smart bypass diode, and  $V_{DS}$  is the voltage drop across the Drain to the Source of a series MOSFET [C1].

To analyze the amount of negative voltage across the shaded cell, an internal structure of a sub-panel is given in Fig. 3.3. For this analysis, various mismatch cases were developed in a publication C1 from which two of such cases are shared in Fig. 3.4. In



**Figure 3.3:** Solar panel with a shaded cell with in a sub-panel: (a) bypass diode and (b) smart bypass diode (SBD) with series-connected MOSFET.



**Figure 3.4:** Current-voltage ( $I$ - $V$ ) characteristics of the PV cell with in a sub-panel equipped with a traditional bypass diode and SBD with series MOSFET at different irradiances: (a) Case 1: 250 W/m<sup>2</sup> and (b) Case 2: 0 W/m<sup>2</sup>.

these two cases, the irradiance over the shaded cell shown in Fig. 3.3 varies from case to case. For the mismatch Case 1, it is 250 W/m<sup>2</sup> and for Case 2, it is 0 W/m<sup>2</sup> while keeping the rest of the irradiance over the other all PV cells at 1000 W/m<sup>2</sup>. The

current-voltage ( $I$ - $V$ ) characteristics curves under these two cases are presented in Fig. 3.4. It can be seen from Fig. 3.4, the negative voltages across the shaded cell for both cases in SBD with series MOSFET solution are lower as compared to traditional bypass diode. Overall, the reduction in the reverse voltage is improved by 16.71% and 16.13% under the irradiances of 250 W/m<sup>2</sup> (Case 1) and 0 W/m<sup>2</sup> (Case 2) for a methodology containing SBD with a series MOSFET with a PV sub-panel, respectively. More detailed analysis and results are presented in a publication C1.

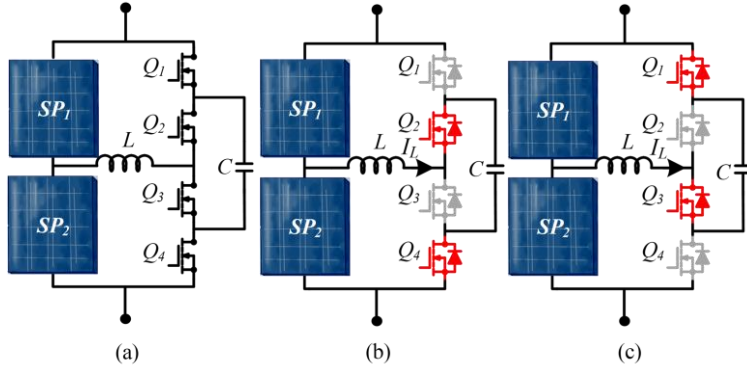
### 3.3. Differential Power Processing (DPP) Solutions

In recent years, various power electronic-based mismatch mitigation topologies have been introduced for solar PV applications. These topologies are commonly known as distributed power electronics-based solutions, which can be integrated easily into the PV cell, sub-panel, and panel-level PV applications due to their smaller sizes. Overall, distributed power electronic topologies helped in the improvement of the performance of solar PV systems under mismatching conditions along with an improvement of PV panel life.

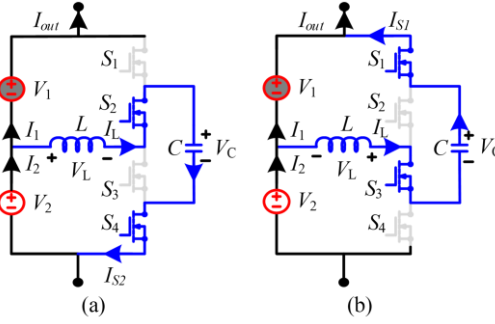
In this section, differential power processing (DPP) converters are explored, which are also typically known as voltage equalizers. Various DPP converters are presented in the literature and some of them are also discussed in Chapter 1. Generally, the DPP converters only process mismatched power or a small amount of power, which is due to the difference between the power generated by solar PV panels that are in series. Additionally, the PV system equipped with DPP converters has only one global peak under mismatching and normal conditions. Therefore, it becomes simple for the MPPT algorithms due to the elimination of multiple power peaks when they are in search of maximum power point (MPP). By considering the advantages of the DPP converter, the two various DPP converters are introduced in C3, C5, and J5, i.e., switched-capacitor-inductor (SCL)- and intrinsic-capacitance-based DPP topologies. These two introduced DPP converters are also discussed in the coming section with some results.

#### 3.3.1. SCL-Based DPP Topology

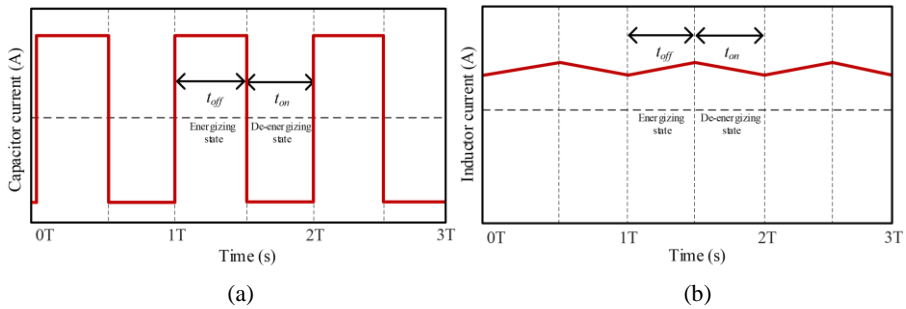
An SCL-based DPP converter is shown in Fig. 3.5. The schematic diagram of the SCL topology is shown in Fig. 3.5(a), which consists of two PV sub-panels represented by  $SP_1$  and  $SP_2$ . For two PV sub-panels, the SCL topology consists of four MOSFET switches ( $Q_1$ ,  $Q_2$ ,  $Q_3$ , and  $Q_4$ ), a capacitor  $C$ , and an inductor  $L$ . The odd-numbered MOSFET switches turned-ON together but complementary to even-numbered switches, as shown in Figs. 3.5(b) and (c), respectively. Moreover, these MOSFETs are switched at a duty ratio of 50%. The capacitor  $C$  and inductor  $L$  are used to process the mismatched power. Additionally, there are two modes of operation where mode 1 is shown in Fig. 3.5(b) and mode 2 in Fig. 3.5(c). In Fig. 3.6, the direction of current is shown during both modes of operation when sub-panel  $SP_1$  is shaded. The timing



**Figure 3.5:** A switched-capacitor-inductor (SCL)-based DPP converter: (a) schematic, (b) mode 1, and (c) mode 2 [C3], [J5].



**Figure 3.6:** Operating modes of switched-capacitor-inductor (SCL)-based DPP converter when  $SP_1$  is shaded: (a) mode 1 and (b) mode 2 [C3], [J5].



**Figure 3.7:** Timing diagram for SCL DPP topology: (a) capacitor current and (b) inductor current.

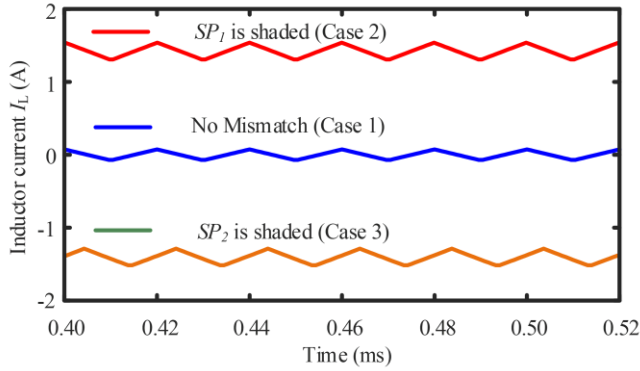
diagram for the capacitor current and inductor current is also shown in Figs. 3.7(a) and (b), which depict the energy store and release in one complete duty cycle time.

**Table 3.1:** Rating of a solar PV sub-panel.

Power at MPP ( $P_{MPP}$ )	45 W
Voltage at MPP ( $V_{MPP}$ )	17.50 V
Current at MPP ( $I_{MPP}$ )	2.58 A
Open-circuit voltage at MPP ( $V_{oc}$ )	22 V
Short-circuit current at MPP ( $I_{sc}$ )	2.86 A

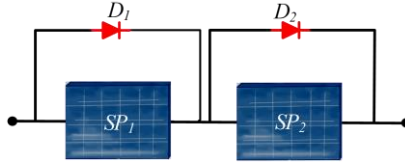
**Table 3.2:** Mismatched cases.

Solar Irradiance	Case 1	Case 2	Case 3
$G_{sp1}$ (W/m <sup>2</sup> )	1000	500	1000
$G_{sp2}$ (W/m <sup>2</sup> )	1000	1000	500

**Figure 3.8:** Mismatch current ( $I_L$ ) through the inductor  $L$  under mismatched cases given in Table 2.2.

To evaluate the performance of the SCL-based DPP topology, simulations were performed in PSIM by using a 45-W PV sub-panel with a specification of that sub-panel is given in Table 3.1. For simulations, various mismatched cases were also developed that are given in Table 3.2. In these mismatched cases, the irradiance ( $G_{sp}$ ) over the PV sub-panels given in 3.5 were varied as depicted in Table 3.2. Moreover, the converter was operating at a 50% duty cycle and 100-kHz frequency. The value of inductor  $L$  and capacitor  $C$  was 100- $\mu$ H and 50- $\mu$ F, respectively. The details of other designed parameters are given in publication C1.

Firstly, the mismatched current that is passing through inductor  $L$  of the circuit in Fig. 3.6 is shown in Fig. 3.8. It can be seen from Fig. 3.8, the value of the current is the same around 1.3A for Cases 1 and 2. However, they are in the opposite direction because the current is flowing in the reverse direction to the referenced current direction.



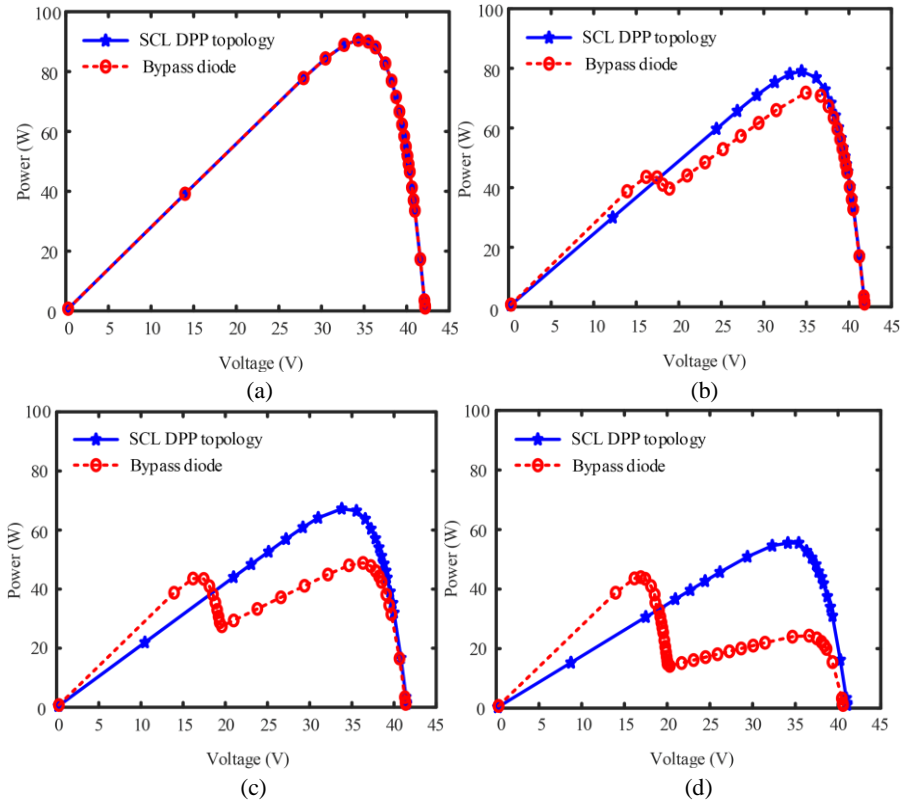
**Figure 3.9:** PV sub-panels with parallel-connected bypass diodes.

**Table 3.3:** Mismatched cases.

Solar Irradiance	Case 1	Case 2	Case 3	Case 4
$G_{sp1}$ (W/m <sup>2</sup> )	1000	750	500	250
$G_{sp2}$ (W/m <sup>2</sup> )	1000	1000	1000	1000

For further evaluation of SCL DPP topology, it was compared with the traditional bypass diode shown in Fig. 3.9. For this purpose, the various mismatched cases were defined, which are shown in Table 2.3 and their results are presented in Fig. 3.10. The results in Fig. 3.10 consist of power-voltage ( $P$ - $V$ ) characteristic curves both for SCL DPP and traditional bypass diode methodology. It can be seen from Figs. 3.10(b)-(d), there are no multiple power peaks for SCL DPP topology whereas there are multiple peaks for bypass diode methodology. Additionally, Fig. 3.10 also depicts that more power is extracted by the SCL DPP topology. Furthermore, the voltages across the PV sub-panels with SCL DPP topology are given in Table 3.4, which are under the mismatched cases presented in Table 3.3. The voltages in Table 3.4 depict the achievement of voltage equalization. More results and details are presented in publications C3 and J5.

In continuation, the experiments were also performed by building a prototype of SCL topology and it was tested in the laboratory, as shown in Fig. 3.11. The experimental setup is shown in Fig. 3.11. The setup detail and procedure of the experiment are explained in publications J5, C3, and C5. For experimentation, two PV panels were used named  $SP_1$  (30-W) and  $SP_2$  (30-W). To create a mismatch, the solar PV sub-panel  $SP_2$  is operating at 90%, 50%, and 25% of  $SP_1$ . In these conditions, the  $P$ - $V$  characteristics curves are shown in Fig. 3.12 and these curves verify the simulated result by eliminating the multiple power peak under mismatch. Similarly, the mismatched current flowing through the inductor  $L$  is shown in Fig. 3.13 under the mismatched cases given in Table 3.5. Overall, from the above discussion, it is shown that by using SCL topology, it is easy to track MPP due to the elimination of multiple peaks. Additionally, the SCL topology is operating at a fixed duty equal to 50%, which makes the topology simple and cost-effective without adding any complex control strategies.



**Figure 3.10:** Power-voltage ( $P$ - $V$ ) characteristic curves under mismatch cases shown in Table 2.3: (a) Case 1, (b) Case 2, (c) Case 3, and (d) Case 4 [J5].

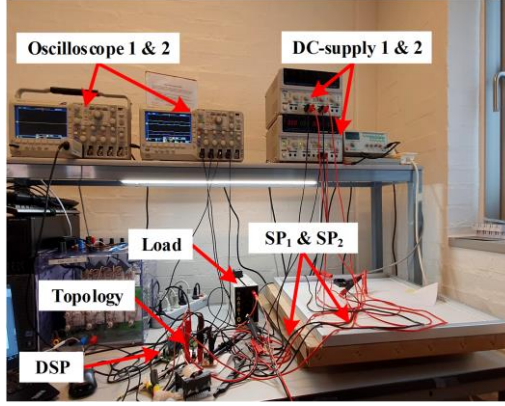
**Table 3.4:** Voltages across the solar PV sub-panels under the mismatched cases given in Table 3.2.

Sub-panel voltages	Case 1	Case 2	Case 3	Case 4
$V_{sp1}$	17.50	17.21	16.89	16.61
$V_{sp2}$	17.50	17.23	16.94	16.68

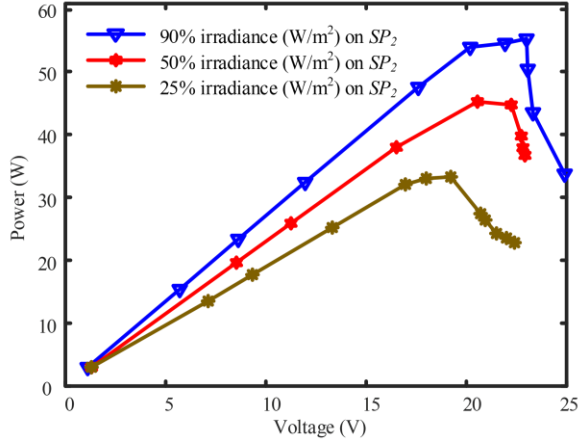
### 3.3.2. Intrinsic-Capacitance-Based DPP Converter Topology for Solar PV Panels

An intrinsic switched-capacitance-based DPP converter topology shown in Fig. 3.14 was presented in a Publication C4. In this topology, the main idea was to unitize the





**Figure 3.11:** Experimental setup [J5].

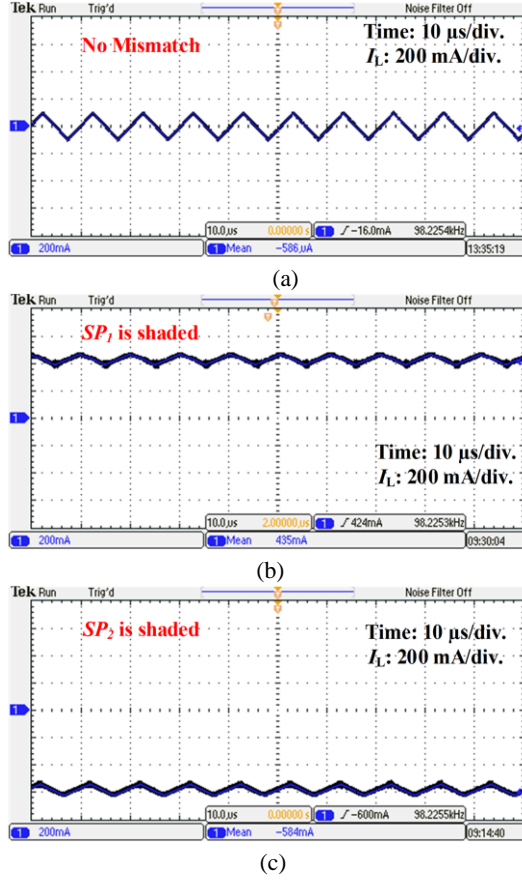


**Figure 3.12:**  $P$ - $V$  characteristics curves from experimentation [J5].

**Table 3.5:** Mismatched cases used for experimentation.

Sub-panel ( $SP_1$ and $SP_2$ )	Case 1	Case 2	Case 3
$I_{sp1}, V_{sp1}$	2, 15	2, 15	1.41, 14.7
$I_{sp2}, V_{sp2}$	2, 15	1.56, 14.8	2, 15

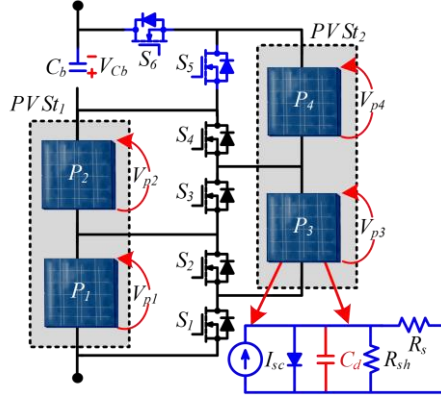
internal capacitance ( $C_d$ ) of the solar PV cell shown in Fig. 3.14, which are in the range of microfarad ( $\mu F$ ) to millifarad ( $mF$ ). The internal capacitance of a PV cell depends on the size of the cell and also depends on the number of cells connected in series. This internal capacitance was used to process the mismatched charges and used as a replacement of external capacitance, which is normally used as in switched-capacitor topologies. The schematic diagram of the intrinsic switched-capacitance topology during modes 1 and 2 is given in Fig. 3.15. During mode 1, the odd number of switches switched ON while even-numbered remained OFF, as shown in Fig.



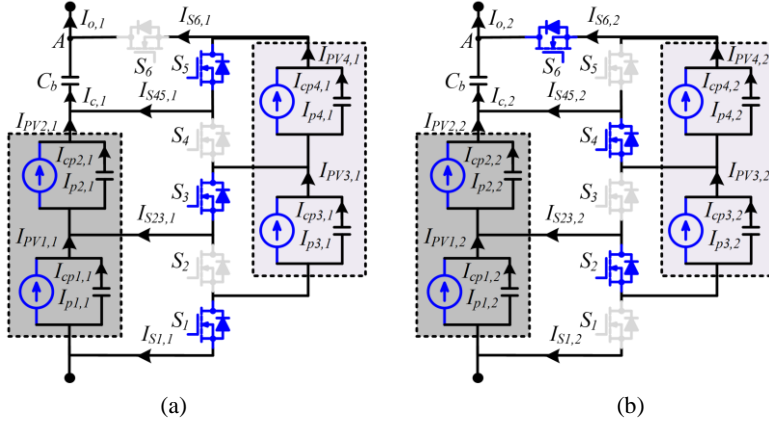
**Figure 3.13:** Mismatched inductor current  $I_L$  through experimental results under mismatch cases given in Table 3.5 [J5].

3.15(a). Similarly, the odd-numbered switches turned OFF and even-numbered turned ON during mode 2, which is shown in Fig. 3.15(b). Overall, in one cycle, the energy is stored by the capacitor  $C_d$  and in the next cycle, the same amount of energy is released by that capacitor. Additionally, the duty cycle of the switches is 50% (fixed) and they are operating at a frequency of 100-kHz.

The intrinsic-capacitance-based DPP converter topology was evaluated through simulations and experimentations by using a 5.01-W PV panel with a maximum voltage ( $V_{mp}$ ) and maximum current ( $I_{mp}$ ) rating of 3.39V and 1.48A, respectively. For this purpose, various mismatch cases were developed for the evaluation of the topology. For simulations, the various three mismatch cases are given in Table 3.6. Here,  $G_{p1}$ ,  $G_{p2}$ ,  $G_{p3}$ , and  $G_{p4}$  are the irradiances over the PV panels ( $P_1$ ,  $P_2$ ,  $P_3$ , and  $P_4$ ). Under these three mismatched cases, the  $P$ - $V$  characteristic curves are presented in Fig. 3.16, which shows the elimination of multiple power peaks issue. Moreover,



**Figure 3.14:** Intrinsic switched capacitor-based DPP converter.



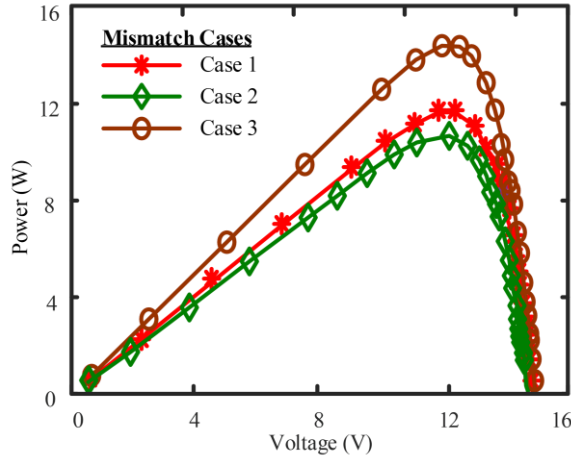
**Figure 3.15:** Intrinsic switched capacitor-based DPP converter: (a) mode 1 and (b) mode 2.

the voltages across the panels ( $V_{p1}$ ,  $V_{p2}$ ,  $V_{p3}$ , and  $V_{p4}$ ) along with overall output voltage ( $V_o$ ) are given in Fig. 3.17 for a mismatch Case 1. The results in Fig. 3.17 show the achievement of voltage equalization under mismatch, which helped in the elimination of mismatch in the PV system by a simple topology shown in Fig. 3.14.

In continuation, the experimental setup is shown in Fig. 3.18 and the procedure of the experiment is briefly described in Publication C4. For evaluation of the topology in Fig. 3.15, various mismatch cases were developed, which are given in Table 3.7. These mismatch cases were created by operating the DC power supplies shown in Fig. 3.18 in common current (CC) mode. The procedure is described in publication C4. The experimental results under these mismatched cases are given in Fig. 3.19, which consist of  $P$ - $V$  characteristic curves. The  $P$ - $V$  characteristics curve shows that there is only one peak under various cases. Additionally, the voltages across the PV panels under these mismatch cases are given in the publication C4 along with the other details containing the simulation and experimental results, and other design parameters that

**Table 3.6:** Mismatched cases [C4].

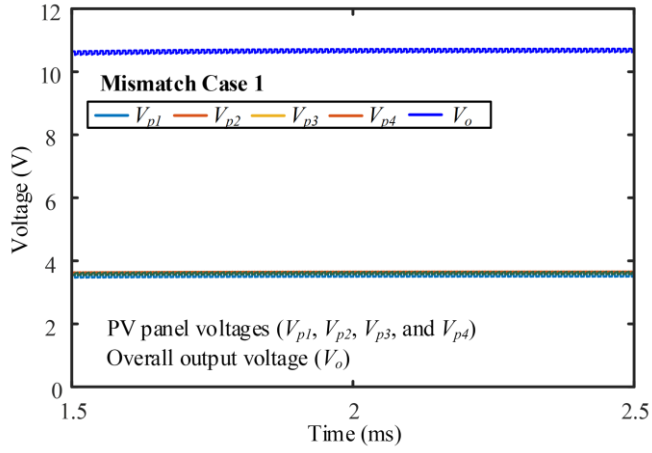
Solar Irradiance	Mismatch Case 1	Mismatch Case 2	Mismatch Case 3
$G_{p1}$ (W/m <sup>2</sup> )	300	500	1000
$G_{p2}$ (W/m <sup>2</sup> )	1000	1000	750
$G_{p3}$ (W/m <sup>2</sup> )	300	500	600
$G_{p4}$ (W/m <sup>2</sup> )	700	200	700

**Figure 3.16:** Power-voltage ( $P$ - $V$ ) characteristic curves under mismatch cases shown in Table 3.6 for a DPP converter in Fig. 3.14 [C4].

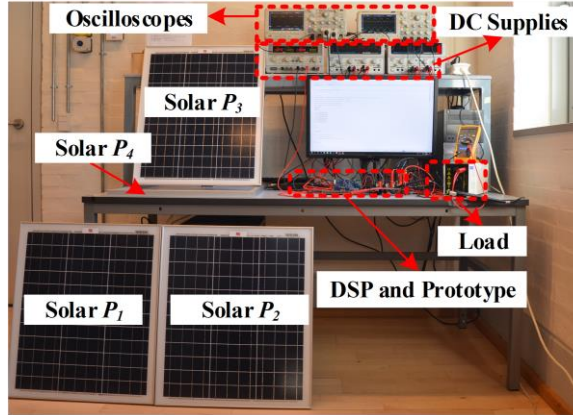
were used during the experimentation and for the verification of the concept.

### 3.4. Comparison between Bypass Diode, DC Optimizers, and DPP Converters

In this section, a comparison between three different methodologies used for mismatch reduction is presented. The three different systems are the bypass diode method shown in Fig. 3.20(a), DC optimizer method in Fig. 3.20(b), and switched-capacitor-based DPP method shown in Fig. 3.20(c). These methodologies were applied at the sub-panel level, as depicted in 3.21. The rating of a PV panel used for the evaluation is given in Table 3.8. The PV panel consists of three sub-panel named  $SP_1$ ,  $SP_2$ , and  $SP_3$ . Each PV sub-panel is comprised of 20 series-connected PV cells, as shown in Fig. 3.21. The mismatch cases that were used for the evaluation of these three topologies under the same conditions are given in Fig. 3.21. The mismatched cases were developed by varying the irradiances over the PV cells. In continuation, in Fig. 3.21, it can be seen that the PV panel consists of three junction points, which were represented as  $T_1$ ,  $T_2$ , and  $T_3$ . Each junction point corresponds to a sub-panel and the topologies shown in Fig. 20 are connected to these junctions.



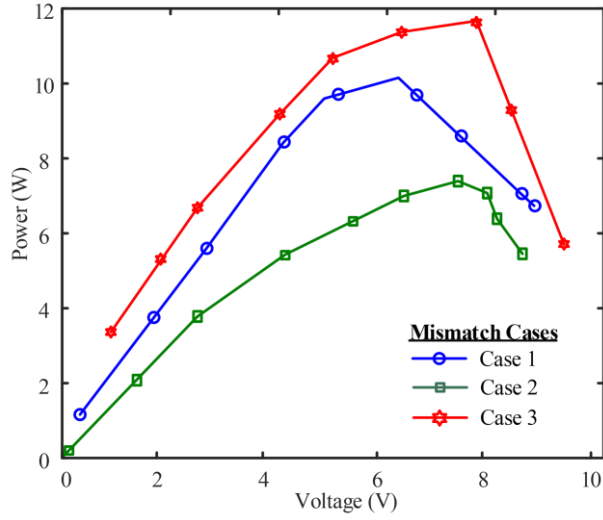
**Figure 3.17:** PV panel voltages under mismatch Case 1 given in Table 3.6 [C4].



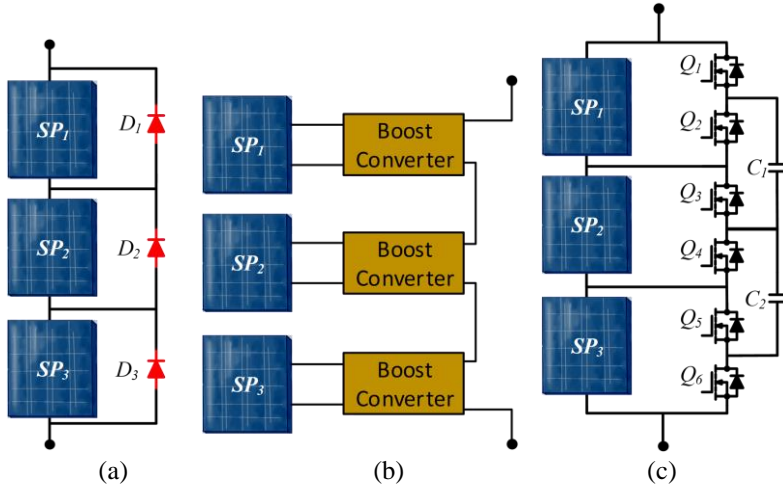
**Figure 3.18:** Experimental setup for intrinsic switched capacitor-based DPP converter [C4].

**Table 3.7:** Mismatched cases for a PV panel shown in Fig. 3.18. Here,  $I_{p1}$ ,  $I_{p2}$ ,  $I_{p3}$ , and  $I_{p4}$  are the currents coming from solar panel P1, P2, P3, and P4, respectively.

Sub-panel currents	Mismatch Case 1	Mismatch Case 2	Mismatch Case 3
$I_{p1}$ (A)	0.36	0.80	1.74
$I_{p2}$ (A)	1.38	1.62	1.30
$I_{p3}$ (A)	0.36	0.84	0.82
$I_{p4}$ (A)	1.03	0.30	1.24



**Figure 3.19:** Experimental results for intrinsic switched capacitor-based DPP converter shown in Fig. 3.18 showing  $P$ - $V$  characteristic curves under various mismatch cases [C4].



**Figure 3.20:** Mismatch reduction methodologies: (a) bypass diode, (b) DC optimizer, and (c) switched-capacitor-based DPP converter.

The results obtained from these three systems are shown in Fig. 20 under various mismatched cases given in 3.22. The results in Fig. 3.22 show the amount of power generated and lost under specific cases by these three methodologies. Considering the mismatch Case 3 in Fig. 3.21, it can be seen that the power generated by the DPP converter was more than the other two topologies because of the low power processing capability of DPP converters. However, in Case 5, the overall power from the DC optimizer was more than the DPP converter and bypass diode because, in the DPP

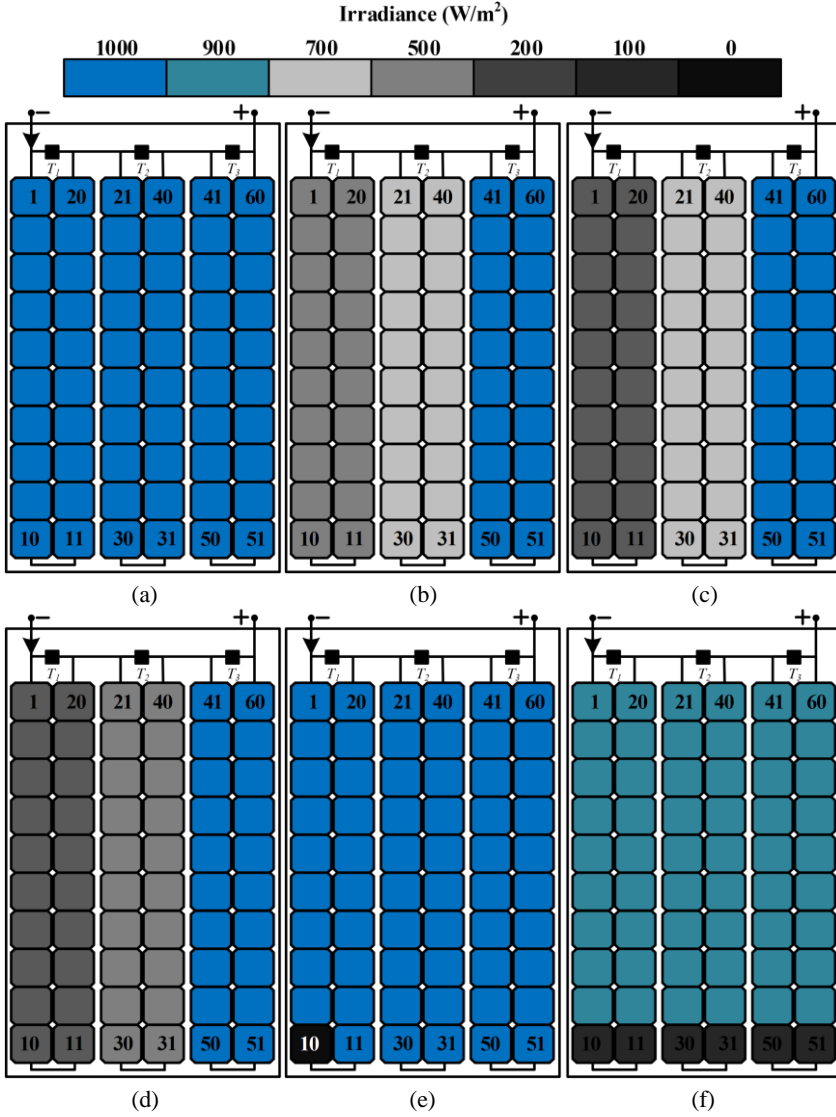
**Table 3.8:** Specification of a PV panel parameters at standard test conditions (STC) for the systems shown in Fig.3.20.

Peak Power ( $P_{\max}$ )	245 W
Voltage at maximum power ( $V_{\text{mp}}$ )	31.30 V
Current at maximum power ( $I_{\text{mp}}$ )	7.84 A
Open-Circuit Voltage ( $V_{\text{oc}}$ )	37.10 V
Short-Circuit Current ( $I_{\text{sc}}$ )	8.48 A

converter, the power is flowing from the bottom to the top like a ladder. Therefore, overall power was affected as one of the PV cells in a sub-panel completely blocks the flow of power, which in turn also affects the power of the other two series-connected PV sub-panels in the case of the DPP converter. Similarly, the PV sub-panel is completely bypassed by a bypass diode in Case 5. Therefore, the power is completely lost from this sub-panel. Additionally, the voltage across the terminal  $T_1$ ,  $T_2$ , and  $T_3$  are given in Table 3.9. More details of PV cell voltages within a sub-panel, other results will be presented in future work. Additionally, the future work will also briefly discusses the comparison among these three methodologies with similar rating five different infield PV systems installed at Politecnico di Milano, Milan, Italy. The comparison will be performed by measuring the real-time irradiances and ambient temperatures.

### 3.5. Summary and Conclusions

This chapter discussed the three different power electronic techniques that were used to reduce or eliminate the effect of mismatch in solar PV systems. The three different techniques were smart bypass diode (SBD) with a series MOSFET, switched-capacitor-inductor (SCL)-based differential power processing (DPP), and intrinsic-capacitance-based DPP converter. The SBD technique used a MOSFET in series with a PV panel, which shares the reverse voltage with the shaded PV cells within the sub-panel. The sharing of voltage reduces the stresses and improves the lifetime of the shaded cell. In continuation, it was shown that the two DPP converters mitigate the mismatch effects in the PV system and also equalize the voltages of all PV cell/sub-panel/panel available in the system. Hence, it eliminates the multiple power peak issues that make a difficult for multiple power point tracking (MPPT) algorithms to track the maximum power point (MPP). Additionally, the DPP converters only process the mismatched power and achieve the ultimate goal with simple circuitry. For evaluation, simulations and experiments were performed to prove the concept by

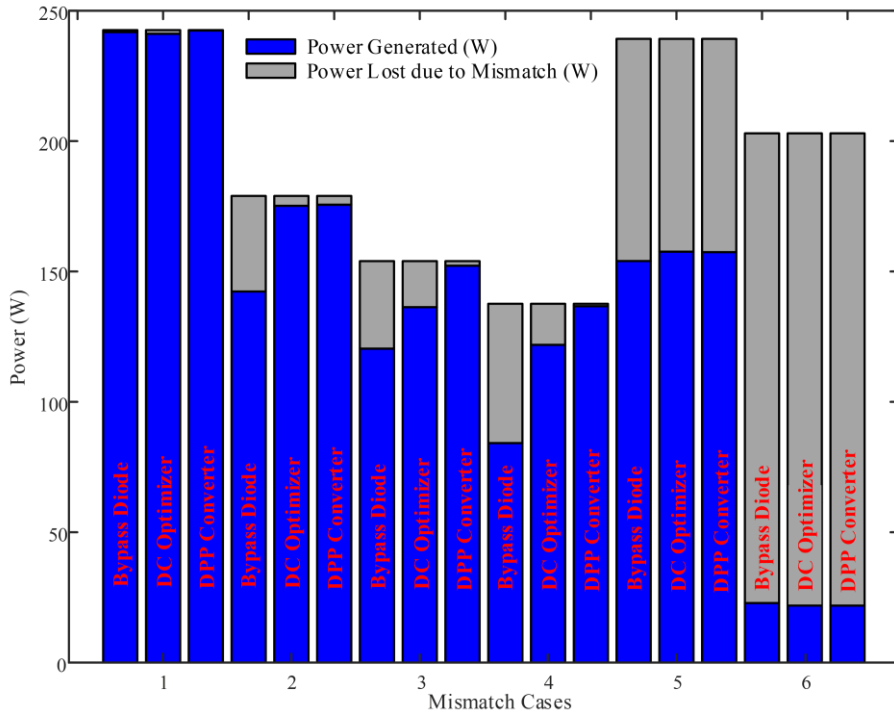


**Figure 3.21:** Mismatch cases: (a) Case 1, (b) Case 2, (c) Case 3, (d) Case 4, (e) Case 5, and (f) Case 6.

considering various mismatch cases. Overall, these techniques helped in the improvement of power extraction from PV systems under non-ideal conditions, e.g., partial shading.

In the last part of this chapter, a comparison between the three various methodologies, i.e., traditional bypass diode, DC optimizers, and DPP converter was discussed in detail. The methods were used to analyze the effectiveness of these three





**Figure 3.22:** Power generated and lost by three different systems shown in Fig. 3.20 under mismatch cases depicted in Fig. 3.21.

**Table 3.9:** Voltage across the PV sub-panels under mismatched cases given in Fig. 3.21.

Mismatch Cases	Bypass diode			DC optimizer			DPP Converter		
	$V_{T1}$	$V_{T2}$	$V_{T3}$	$V_{T1}$	$V_{T2}$	$V_{T3}$	$V_{T1}$	$V_{T2}$	$V_{T3}$
Case 1	10.37	10.37	10.37	10.22	10.22	10.22	10.18	10.18	10.18
Case 2	8.84	11.62	12.30	10.40	10.27	10.55	10.19	10.42	10.62
Case 3	-0.7	9.79	11.72	-0.0007	10.38	10.38	9.50	10.05	10.27
Case 4	-0.7	10.54	12.41	-0.004	10.35	10.35	9.40	9.79	10.16
Case 5	-0.7	10.56	10.56	-0.0017	10.42	10.42	8.44	10.01	10.13
Case 6	-0.7	10.33	10.33	0.001	10.21	10.21	9.17	9.94	10.16

methodologies under various commonly existed mismatched conditions by considering real system specifications installed at Politecnico di Milano, Milan, Italy. In the end, the developed models were also compared by the real systems by considering the real irradiance profiles and ambient temperatures. Overall, the results show that DPP converters perform better than the other two methodologies in a silent mismatch. However, if the PV cell or sub-module is completely shaded then it affects the performance of DPP converters. In such cases, the DC optimizers are better. However, the reverse voltage stresses across the shaded PV cells within a sub-panel were greatly reduced when using DPP converters. Finally, if there is no mismatch then bypass diode is the best solution due to lower cost, simplicity, and size.

# CHAPTER 4.

## 4. Integration of Differential Power Processing (DPP) Converters in Solar PV Interconnection Schemes

Many research efforts have been made to improve the performance of solar PV systems under partial shading and other mismatch conditions by presenting various power-electronic-based solutions for the series-connected PV panels. The DPP converters are one of them, which are used for mismatch mitigation as discussed in the previous section. However, these DPP topologies are not explored for parallel-connected PV strings where each string consists of several series-connected PV panels. Therefore, this section presents the study of DPP topologies by integrating them with parallel-connected PV strings. In continuation, this chapter also explores the various PV string interconnection schemes, e.g., series-parallel (SP), total-cross-tied (TCT), central-cross-tied (CCT), and bridge-linked (BL) by integrating a DPP topology with these schemes. These inter-connection schemes are explored with DPP technology under various mismatch scenarios. Afterward, they are also compared with similar systems equipped with the state-of-the-art method, i.e., bypass diode method.

### 4.1. Introduction

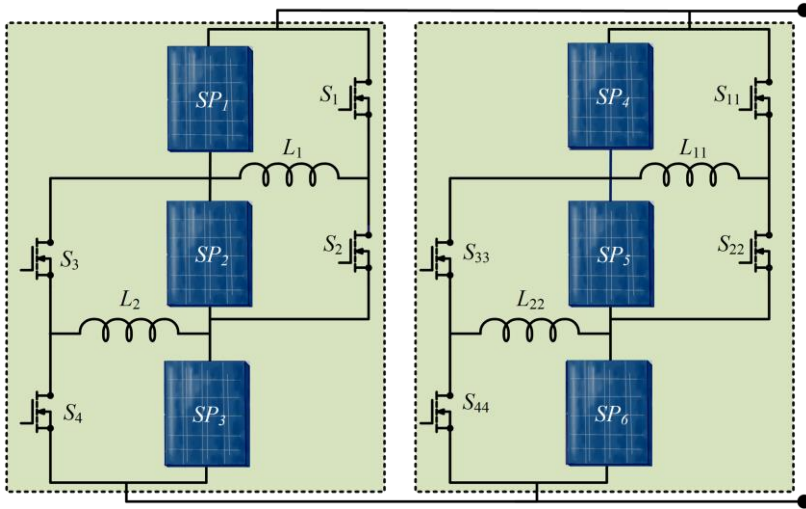
The first part of this chapter deals with a parallel connection of PV strings. In this study, two different DPP topologies are considered for the analysis in two different works. In the first work, a switched-inductor (SL)-based DPP topology is used and the switched-capacitor (SC) DPP topology is used in the second work. The results under various mismatch scenarios show a significant improvement in the overall output power extracted from the PV systems in comparison to traditional bypass diode methodology. The discussion of these methodologies is presented in the publications C2 and C5.

In the second part of this chapter, the DPP converters are also analyzed on various PV string inter-connection schemes, which include SP, TCT, CCT, and BL. For analysis, various shading scenarios are considered such as one-panel, short-wide, long-narrow, central, and diagonal shading. Under these shading patterns, the above-mentioned interconnection schemes equipped with DPP converters are compared with similar systems that are equipped with traditional bypass diodes under the same shading patterns. The results and discussion of this work are presented in a publication J2.

## 4.2. Switched-Inductor-Based DPP Architecture in Parallel-Connected PV Strings

In this section, a switched-inductor (SL)-based DPP topology was used for PV strings that were connected in parallel, as shown in Fig. 4.1. The concept was introduced in a publication C2. In this work, two parallel-connected PV strings, each containing three series-connected PV sub-panels ( $SP_1$ ,  $SP_2$ ,  $SP_3$ ,  $SP_4$ ,  $SP_5$ , and  $SP_6$ ) were equipped with SL DPP topology, as shown in Fig. 4.1. In this SL-based DPP topology, the odd-numbered switches ( $S_1$ ,  $S_3$ ,  $S_{11}$ , and  $S_{33}$ ) and even number switches ( $S_2$ ,  $S_4$ ,  $S_{22}$ , and  $S_{44}$ ) turned ON and OFF alternatively at a 50% duty cycle. The operating frequency of these switches was 100 kHz. The detailed design and operational principles are given in a publication C2.

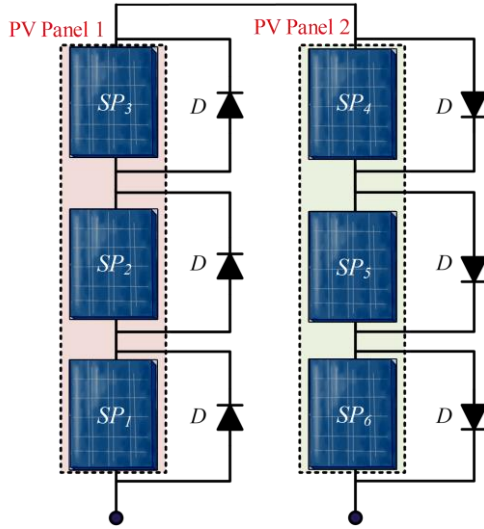
The mismatched cases that were used for the analysis of the topology are given in Table 4.1. In total, six mismatched cases were developed by varying the irradiances over the PV sub-panels. The irradiance over the PV sub-panels  $SP_1$ ,  $SP_2$ ,  $SP_3$ ,  $SP_4$ ,  $SP_5$ , and  $SP_6$  are  $G_{sp1}$ ,  $G_{sp2}$ ,  $G_{sp3}$ ,  $G_{sp4}$ ,  $G_{sp5}$ , and  $G_{sp6}$ , respectively, as depicted in Table 4.1. The system shown in Fig. 4.1, which is equipped with SL DPP was compared with a PV system containing six PV sub-panels connected in series equipped with parallel-connected traditional bypass diodes for performance comparison, as shown in Fig. 4.2. The rating of each sub-panel was 60 W at standard test conditions (STC) with a maximum current ( $I_{max}$ ) and voltage ( $V_{max}$ ) of 3.50 A and 17.10 V, respectively. The results under mismatched cases given in Table 4.1 are presented in Fig. 4.3. Fig. 4.3 depicts the power extraction from SL DPP and bypass diode architecture. For example, it can be seen from Fig. 4.3, the power extracted by SL DPP architecture is



**Figure 4.1:** Switched-inductor (SL)-based DPP topology in parallel-connected PV strings [C2].

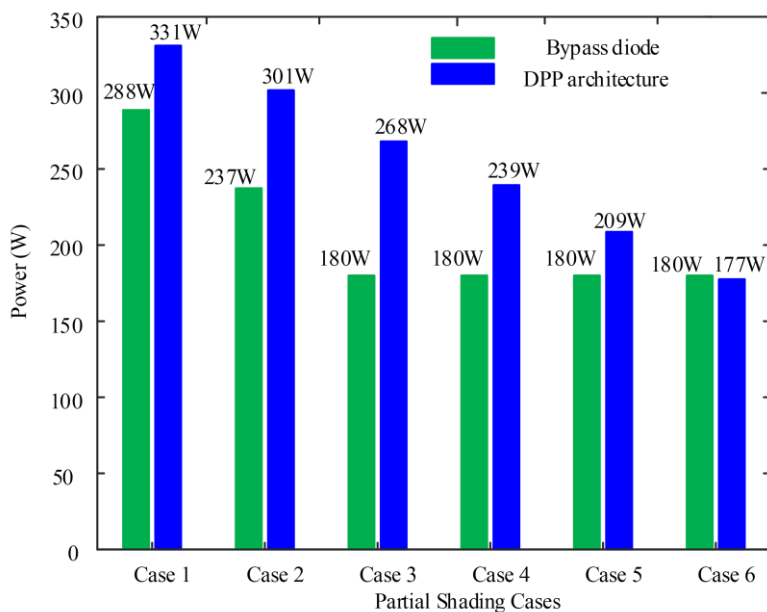
**Table 4.1:** Partial shading cases for PV sub-panels shown in Figs. 4.1:  $SP_1$ ,  $SP_2$ ,  $SP_3$ ,  $SP_4$ ,  $SP_5$ , and  $SP_6$ .

Irradiance ( $\text{W}/\text{m}^2$ )	Case 1	Case 2	Case 3	Case 4	Case 5	Case 6
$G_{sp1}$	500	500	500	500	500	500
$G_{sp2}$	1000	500	500	500	500	500
$G_{sp3}$	1000	1000	500	500	500	500
$G_{sp4}$	1000	1000	1000	500	500	500
$G_{sp5}$	1000	1000	1000	1000	500	500
$G_{sp6}$	1000	1000	1000	1000	1000	500



**Figure 4.2:** PV panel with three series-connected PV sub-panels equipped with parallel-connected bypass diodes.

268 W and 239 W under mismatch cases 3 and 4, respectively. However, in the case of using standard bypass diodes, it is 180 W for both mismatched cases 3 and 4 because the low-power-producing PV sub-panels were bypassed by their bypass diodes. It can be seen from the results that the DPP architecture extracts much more power as compared to bypass diode in parallel string connections. Additionally, the voltages across the PV sub-panels under these mismatched cases are also given in Table 4.2, which shows that a voltage equalization was achieved by using the DPP methodology in parallel string connections. In Table 4.2,  $V_{SP1}$ ,  $V_{SP2}$ ,  $V_{SP3}$ ,  $V_{SP4}$ ,  $V_{SP5}$ , and  $V_{SP6}$  are the voltages across the sub-panels  $SP_1$ ,  $SP_2$ ,  $SP_3$ ,  $SP_4$ ,  $SP_5$ , and  $SP_6$ ,



**Figure 4.3:** Results showing the output power extract by DPP architecture shown in Fig. 4.1 and bypass diode architecture in Fig. 4.2 under mismatch cases given in Table 4.1.

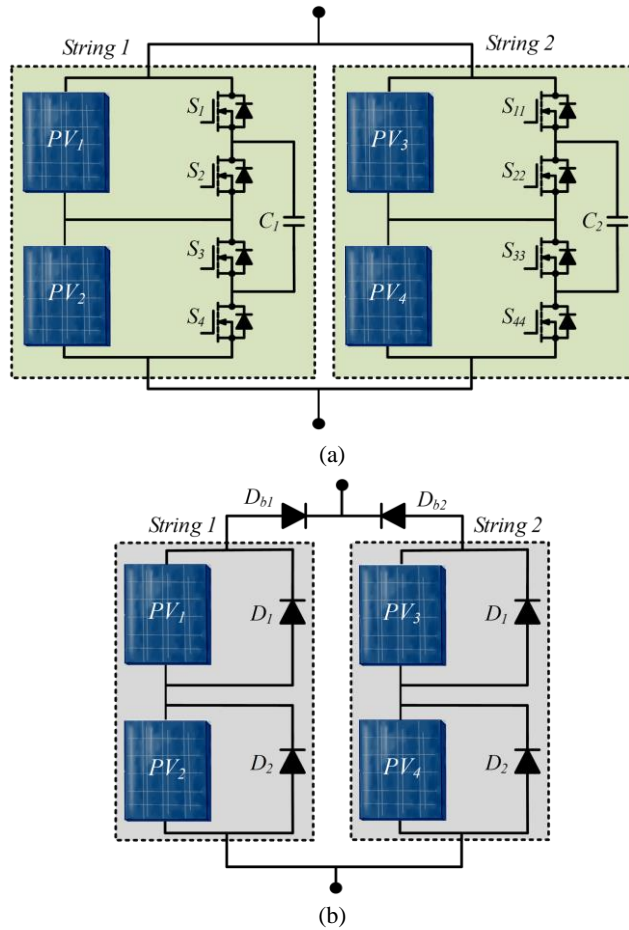
**Table 4.2:** Voltage across PV sub-panels during various cases when panels are equipped with SL DPP [C2].

Cases	$V_{SP1}$ (V)	$V_{SP2}$ (V)	$V_{SP3}$ (V)	$V_{p1}$ (V)	$V_{SP4}$ (V)	$V_{SP5}$ (V)	$V_{SP6}$ (V)	$V_{p2}$ (V)
Case 1	17.03	17.03	17.03	51.09	17.03	17.03	17.03	51.09
Case 2	16.80	17.10	17.02	50.2	17.00	17.00	17.00	51
Case 3	16.60	16.80	17.00	50.4	16.80	16.80	16.80	50.04
Case 4	17.10	17.10	17.10	51.3	16.90	17.10	17.10	51.1
Case 5	17.01	17.02	17.02	51.05	16.85	16.99	17.09	50.93
Case 6	16.31	16.32	16.32	48.95	16.31	16.32	16.32	48.95

respectively. Additionally,  $V_{p1}$  and  $V_{p2}$  in Table 4.2 are the voltages across the two parallel-connected PV strings named PV panel 1 and PV panel 2, respectively. More results and discussions are presented in a publication C2.

### 4.3. Switched-Capacitor-Based DPP Architecture in Parallel-Connected PV Strings

In this section, a switched-capacitor (SC)-based DPP topology was used for parallel-connected PV strings, as shown in Fig. 4.4(a). The concept was introduced in a publication C5. In this work, two parallel-connected PV strings, each containing two series-connected PV panels ( $PV_1$ ,  $PV_2$ ,  $PV_3$ , and  $PV_4$ ) were equipped with SC topology as shown in Fig. 4.4(a). In this SC-based DPP topology, the odd-numbered MOSFET switches ( $S_1$ ,  $S_3$ ,  $S_{11}$ , and  $S_{33}$ ) and even-numbered MOSFET switches ( $S_2$ ,  $S_4$ ,  $S_{22}$ , and  $S_{44}$ ) turned ON and OFF alternatively at a 50% duty cycle. The operating frequency of these switches was 100 kHz. The detailed design and operational principles are given in publication C5.



**Figure 4.4:** Schematics of parallel-connected PV strings: (a) switched-capacitor (SC) DPP topology and (b) bypass diode topology [C5].

For performance evaluation, the system that is shown in Fig. 4.4(a), which is equipped with SC DPP was compared with a similar PV system containing two PV strings. Each PV string consists of two series-connected PV panels ( $PV_1$ ,  $PV_2$ ,  $PV_3$ , and  $PV_4$ ) and these PV panels consist of parallel-connected bypass diodes ( $D_1$ ,  $D_2$ ,  $D_3$ , and  $D_4$ ), as shown in Fig. 4.4(b). The rating of the under-test PV panels is given in Table 4.3. In continuation, for evaluation, several mismatched cases were developed, which are given in Table 4.4. In total, five mismatched cases were developed by varying the irradiances over the PV panels. The irradiance over the PV panels  $PV_1$ ,  $PV_2$ ,  $PV_3$ , and  $PV_4$  are  $G_{sp1}$ ,  $G_{sp2}$ ,  $G_{sp3}$ , and  $G_{sp4}$ , respectively as depicted in Table 4.4.

**Table 4.3:** Ratings of the PV panel under test [C2].

Parameter	Value
Rated Maximum Power ( $P_{\max}$ )	60 W
Voltage at maximum power ( $V_{\text{mp}}$ )	17.10 V
Current at maximum power ( $I_{\text{mp}}$ )	3.50 A
Open-Circuit Voltage ( $V_{\text{oc}}$ )	21.10 V
Short-Circuit Current ( $I_{\text{sc}}$ )	3.80 A

The results under the mismatched cases given in Table 4.4 are presented in Fig. 4.5. In Fig. 4.5(a), the power extracted by SC DPP and bypass diode architecture is shown. It can be seen from Fig. 4(a), the power extracted by the SC DPP architecture is more than in the case of a PV panel with only a bypass diode. For the mismatched cases 2-4, the power extracted when using the bypass diode was constant due to the bypassing of the low-power-producing PV panels. Additionally, the  $P$ - $V$  characteristic curves are also presented in Fig. 4.5(b). Fig. 4.5(b) shows the elimination of multiple power peaks, which are caused by the partial shading, and other non-idealities is now removed by the SC DPP topology when it is integrated with parallel-connected PV strings. Overall, the SC DPP architecture in parallel-connected PV strings extracts much more power as compared to bypass diode with these parallel strings. Additionally, the voltage across the PV panels was also equalized. More results and discussions are presented in publication C5.

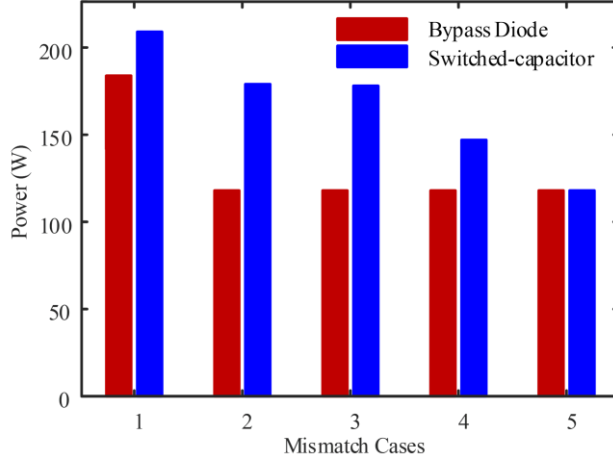
#### 4.4. DPP Architecture in PV String Interconnection Schemes

Various works have been presented in the literature to improve the performance and energy extraction from solar PV systems under partial shading. For this purpose, various interconnection schemes were explored that helped in the improvement of energy extraction. The most commonly used techniques are series-parallel (SP), total-cross-tied (TCT), central-cross-tied (CCT), and bridge-linked (BL), which were

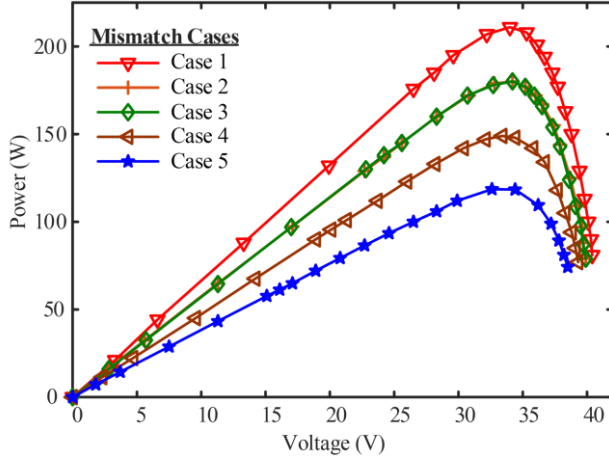


**Table 4.4:** Partial shading cases.

Irradiance (W/m <sup>2</sup> )	Case 1	Case 2	Case 3	Case 4	Case 5
$G_{sp1}$	500	500	1000	500	500
$G_{sp2}$	1000	500	500	500	500
$G_{sp3}$	1000	1000	500	500	500
$G_{sp4}$	1000	1000	1000	1000	500

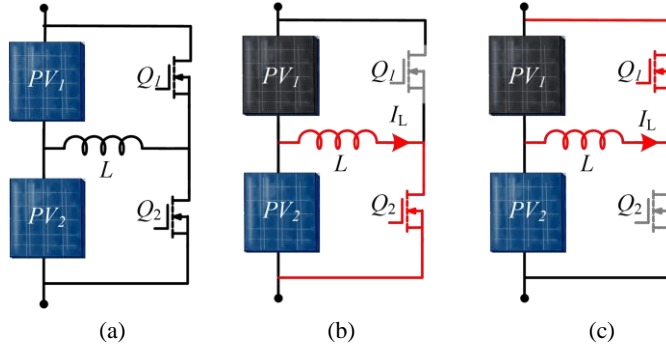


(a)

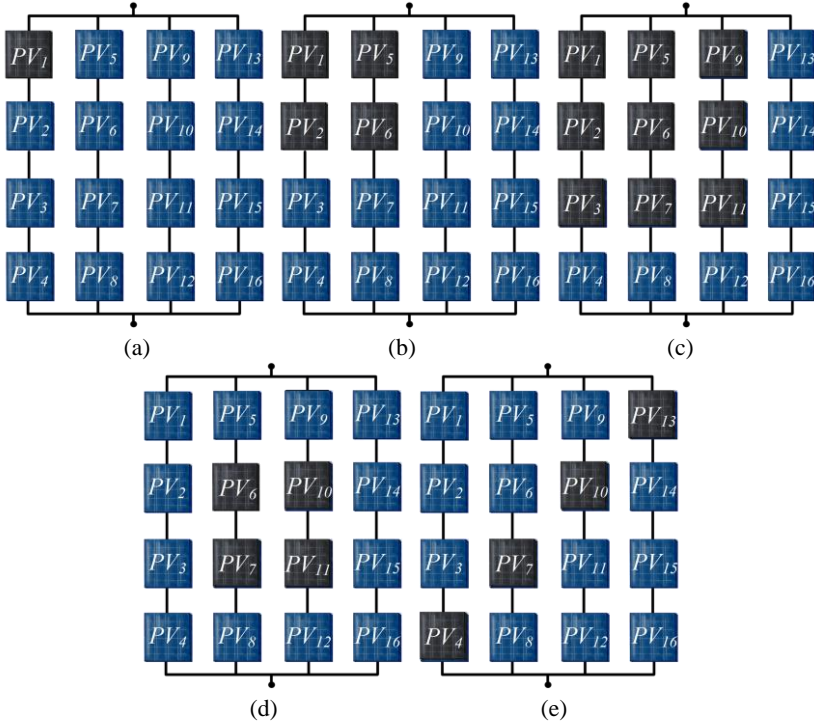


(b)

**Figure 4.5:** Simulated results: (a) output power of the panels with traditional bypass diode and SC DPP topology and (b) power-voltage ( $P$ - $V$ ) characteristic curves for the proposed architecture under mismatch cases given in Table 4.4.

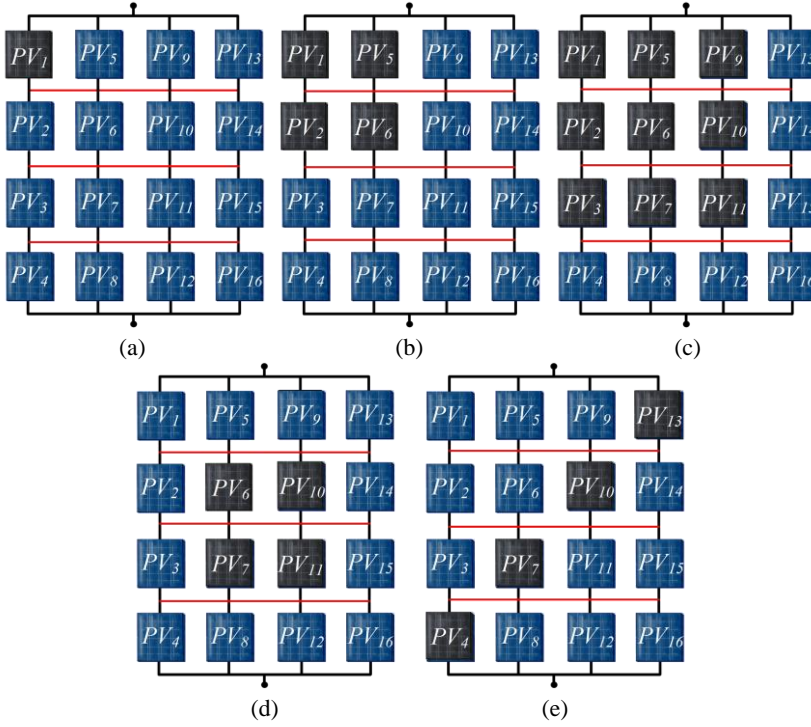


**Figure 4.6:** Switched-inductor (SL)-based DPP architecture: (a) general schematic, (b) MOSFET  $Q_2$  is ON and  $Q_1$  is OFF, and (c) MOSFET  $Q_2$  is ON and  $Q_1$  is OFF [J2].



**Figure 4.7:** Series-parallel (SP) connection with different shading patterns: (a) one-panel, (b) short wide, (c) long narrow, (d) central shading, and (e) diagonal shading [J2].

shown in Fig. 1.12, Chapter 1. These interconnection schemes were previously studied by using a bypass diode methodology to minimize the partial shading and other non-ideal effects. However, in Publication J2, the SL-based DPP converter topology was integrated with these interconnection schemes to analyze the behavior and performance of the overall PV system, as shown in Fig. 4.6.



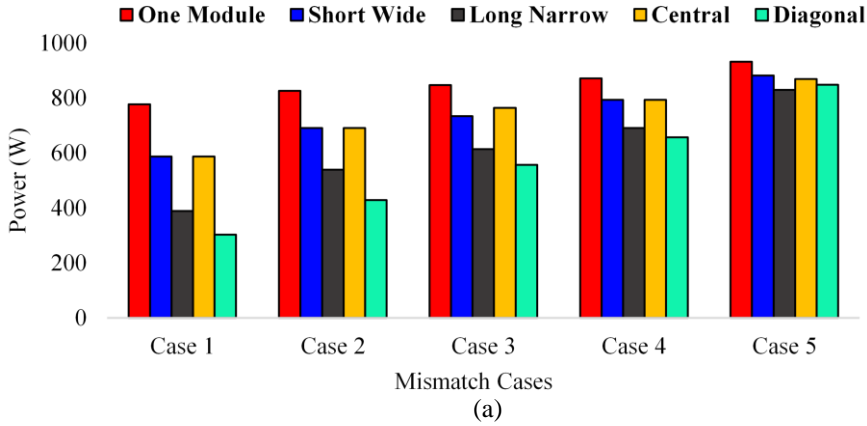
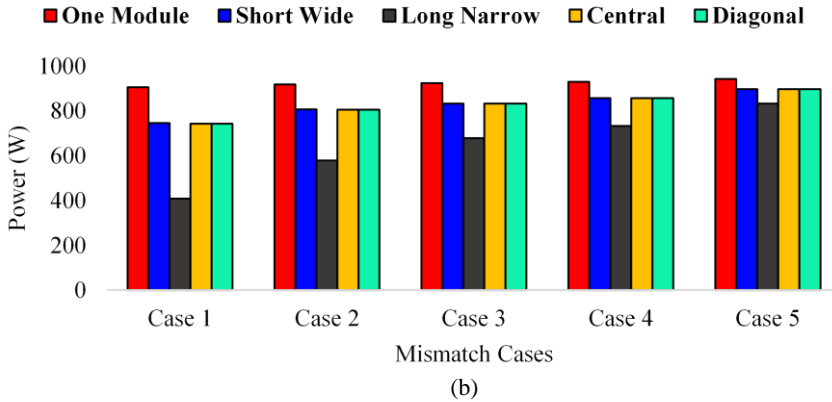
**Figure 4.8:** Total-cross-tied (TCT) connection with different shading patterns: (a) one-panel, (b) short wide, (c) long narrow, (d) central shading, and (e) diagonal shading [J2].

To integrate DPP converters with different string interconnection schemes, a 4x4 PV array was considered, as shown in Fig. 1.12. These interconnection schemes were evaluated by considering various shading patterns, i.e., one-panel shading in Figs. 4.7-4.8(a), short wide shading in Figs. 4.7-4.8(b), long narrow shading in Figs. 4.7-4.8(c), central shading in Figs. 4.7-4.8(d), and diagonal shading in Figs. 4.7-4.8(e). A 60 W solar PV panel was used during the analysis. The detailed rating of the PV panels is given in Table 4.3.

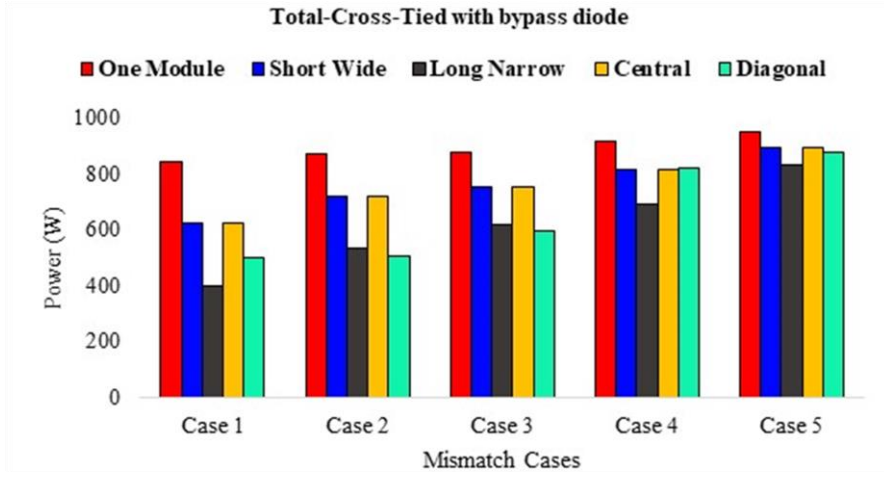
The performance of the above-mentioned interconnection schemes that were equipped with SL DPP topology was evaluated under several mismatched cases given in Table 4.5. In these mismatched cases, the irradiances ( $G$ ) were varied over the panels in the 4x4 PV array system. Hence, each shading pattern, which is shown in Figs. 4.7 and 4.8 further consist of several mismatched cases by varying the irradiance. Additionally, the interconnection systems with SL DPP converters were also compared with similar traditional PV systems that were equipped with parallel-connected bypass diodes to evaluate the performance of the proposed concept given in publication J2. Some of the results in publication J2 under the mismatched cases in Table 4.5 for SP and TCT interconnection schemes are presented in Figs. 4.9 and 4.10,

**Table 4.5:** Mismatch Cases [J2].

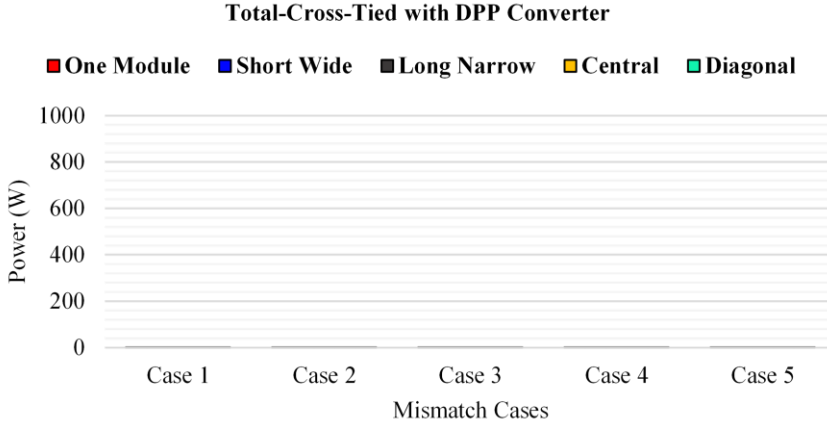
Mismatch Cases	Case 1	Case 2	Case 3	Case 4	Case 5
$G$ (W/m <sup>2</sup> )	200	400	500	600	800

**Series-Parallel-Connection with bypass diode****Series-Parallel-Connection with DPP Converter****Figure 4.9:** Power generated under specific shading patterns and mismatch cases given in Table 4.5 for SP interconnection scheme: (a) bypass diode and (b) SL DPP topology [J2].

respectively. In Fig. 4.9, the power extracted by SP connection for SL DPP and bypass diode architecture is presented. The results show that under various mismatched cases the DPP architecture extracts much more power than the case with only the bypass diode method. However, in Fig. 4.10, the power extracted by TCT connection containing DPP architecture is almost zero because the connections in SL DPP with TCT disturb the working principle of the integrated DPP topology. Therefore, the



(a)



(b)

**Figure 4.10:** Power generated under specific shading patterns and mismatch cases given in Table 4.5 for TCT interconnection scheme: (a) bypass diode and (b) SL DPP topology [J2].

output power extracted by the DPP topology in TCT connections is almost zero. Hence, DPP topology does not apply to the TCT connection scheme. Similarly, it is also not applicable to the BL interconnection scheme. The more detailed discussion and results are presented in the publication J2.

#### 4.5. Summary and Conclusions

This chapter discussed the use of DPP converters in various interconnection schemes, i.e., series-parallel (SP), total-cross-tied (TCT), central-cross-tied (CCT), and

bridged-link (BL). The switched-inductor (SL) and switched-capacitor (SC)-based DPP converter topologies were used in these PV system interconnection schemes to analyze the effect of mismatch. For this purpose, various PV system models were developed and used for the analysis. In the first part of the chapter, a system consisting of two parallel-connected PV strings was considered. In this system, both SL and SC DPP topologies were used to analyze the performance.

In the second part of the chapter, the SL topology was considered for the 4x4 PV systems, which were connected in four various interconnection schemes, i.e., SP, TCT, CCT, and BL. These systems were evaluated under different shading patterns, which include one-panel, short wide, long narrow, central, and diagonal shading patterns. In these shading patterns, various mismatch cases were developed by varying the irradiances over the system. In the end, the result of these systems was compared with the traditional bypass diode method. The results showed and confirmed that it is not possible to integrate the DPP converter topologies to TCT and BL interconnection schemes because of the internal PV panel connections. However, in SP and CCT, the performance of DPP converters is better than the bypass diode. Moreover, the PV panels in these topologies also achieve voltage equalization, which helped in the elimination of multiple power peaks in the  $P$ - $V$  characteristic curves of the system. Overall, it is possible to integrate the DPP converter to the most commonly used PV connection scheme, i.e., SP connection, which consists of parallel-connected PV strings and their performance is better than the traditional systems, which are equipped with bypass diodes. However, the DPP converter with interconnection schemes will increase the cost and complexity of the system.

# CHAPTER 5.

## 5. Conclusions

The main outcomes and contributions of the Ph.D. study – *Mismatch effects and their mitigation techniques in the solar photovoltaic system*, are summarized in this chapter. Additionally, several recommended research areas are also demonstrated at the end for future work.

### 5.1. Thesis Contributions and Outcomes

This Ph.D. thesis investigated the various *mismatch effects, their causes in different PV panel technologies, and finally proposed various solutions to mitigate or reduce these mismatch effects in the solar PV system*. A summary of this Ph.D. thesis is presented as follows.

**In Chapter 1**, the introduction of the Ph.D. thesis is provided, where the background of the research topic and the objective of the Ph.D. study were discussed. The Ph.D. project deals with the study of mismatch effects and various solutions to mitigate these effects. Following these, the research objectives and limitations faced during the Ph.D. project were also outlined in this Chapter.

**Chapter 2** studied the mismatch effects and their causes in a solar PV system by considering different panel technologies, i.e., c-Si and thin-film PV panels. The electrical parameters and thermographic images were analyzed both for c-Si and thin-film PV panels. The analysis depicted that both panel technologies behaved differently under various mismatch conditions and the effect of mismatch were much worse on c-Si panels. Overall, this work helped in a better understanding of panel technologies under non-ideal environmental conditions.

Additionally, a machine-learning (ML)-based diagnostic method was proposed, which used nBayes ML classification technique. The nBayes technique used the texture and HOG features for the classification of c-Si solar thermal images into three categories, i.e., NDH, NDNH, and defective by achieving an efficiency of 94.10%.

**In Chapter 3**, three power electronics-based mismatch mitigation solutions were presented. The three different solutions were smart bypass diode (SBD) with a series MOSFET, switched-capacitor-inductor (SCL)-based differential power processing (DPP), and intrinsic-capacitance-based DPP converter. From these above-mentioned solutions, the SBD not only minimized the mismatched or partial shading effect but also minimized the stresses over the shaded PV cell within a PV sub-panel. Therefore, SBD is a simple and cheap solution that can be used to improve the performance and

life of the overall system. However, the proposed DPP converter solutions eliminate the non-ideal effects in the PV system along with the elimination of the multiple power peak issues that make a difficult for multiple power point tracking (MPPT) algorithms to track the maximum power point (MPP). Therefore, if the cost is not an issue and performance along with the life of the system is more important then the proposed DPP techniques are preferable as they are simple and easily integrable.

In continuation, the traditional bypass diode, DC optimizers, and DPP converter were compared in this chapter by developing a PV system model. The developed model used the real irradiance profiles and ambient temperatures for evaluation under real conditions. This comparison study helped in the selection of the best suitable solution under various non-ideal environmental conditions.

Finally, in **Chapter 4**, the commonly available DPP converters were integrated with PV panels or sub-panels in different PV array inter-connection schemes, e.g., SP, TCT, CCT, and BL. This research study analyzed the possibility of integration of DPP converters in the above-mentioned interconnection schemes. From the analysis, it was concluded that not all interconnection schemes are simple to integrate with DPP converters. because of internal electrical connections. However, it was found that these DPP converters can be integrated with SP and CCT interconnection schemes and they performed better than the traditional PV systems, which are equipped with parallel-connected bypass diodes.

## **5.2. Future Work**

This Ph.D. project has contributed with several findings and resulted in many publications. However, there is a possibility to extend this work in various directions. The further research dimensions that could be exciting and interesting to be inquired are listed as follows:

### **Mismatch effects on bifacial solar PV panel technology**

Mismatch study was only considered for crystalline-silicon (c-Si) and thin-film PV panel technologies. Nevertheless, there are other PV panel technologies, which are becoming more popular due to their high conversion efficiency, e.g., bifacial solar PV panels. Bifacial solar PV panels produce power from both sides, i.e., front and back. Therefore, the study of the bifacial solar PV panels can be an interesting area to explore by introducing various mismatch scenarios.

### **PV panel defect diagnosis using electroluminescence (EL) imaging**

A machine-learning-based diagnostic methodology that was used in this work can be further explored for the detection of various internal defects in the solar panels by using EL images, e.g., cracks in cells, bus bar damage. In addition, deep learning methods can also be used to improve defect diagnostics both using IR and EL images.



Additionally, the quality of the data can also help in the improvement of results, which were achieved in this work using nBayes classifier.

### **Mismatch detection methods**

Power electronics-based mismatch detection algorithms can be proposed that helped in the detection of mismatch by using various electrical parameters to prevent continuous switching of power electronic devices. In this way, switching losses can be improved.

Additionally, the reliability of the proposed converters was not studied. Therefore, its dynamic analysis will be an interesting area to analyze the life of the converter by introducing various stresses that are expected in real scenarios.

### **Integration of differential power processing (DPP) converters in solar PV interconnection schemes**

The integration of DPP converters with real PV string interconnection systems can be explored to analyze the real PV system performance. Additionally, DPP converters can also be used to introduce new dynamic reconfiguration techniques.



# BIBLIOGRAPHY

## References

- [1] REN21. “*Renewable Energy Policy Network for the 21st Century Renewables 2017*,” Global Status Report—REN21; REN21: Paris, France, 2017; pp. 1–302.
- [2] E. Çakırlar Altuntaş and S. L. Turan, “Awareness of secondary school students about renewable energy sources\*,” *Renewable Energy*, vol. 116, pp. 741–748.
- [3] C. Candelise, M. Winksel, and R. J. K. Gross, “The dynamics of solar PV costs and prices as a challenge for technology forecasting,” *Renewable and Sustainable Energy Reviews*, vol. 26, pp. 96–107, Oct. 2013.
- [4] The International Energy Agency (IEA). “*2018 Snapshot of Global Photovoltaic Markets*,” IEA: Paris, France, 2018.
- [5] The International Energy Agency (IEA), “*2018 Photovoltaic Module Energy Yield Measurements: Existing Approaches and Best Practice*,” IEA: Paris, France, 2018.
- [6] S. M. Ahsan and H. A. Khan, “Performance comparison of CdTe thin film modules with c-Si modules under low irradiance,” *IET Renewable Power Generation*, vol. 13, no. 11, pp. 1920–1926, May 2019.
- [7] H. Ali and H. A. Khan, “Techno-economic evaluation of two 42 kWp polycrystalline-Si and CIS thin-film based PV rooftop systems in Pakistan,” *Renewable Energy*, vol. 152, pp. 347–357, Jun. 2020.
- [8] A. J. Carr and T. L. Pryor, “A comparison of the performance of different PV module types in temperate climates,” *Solar Energy*, vol. 76, no. 1, pp. 285–294, Jan. 2004.
- [9] Y. Yang, K. A. Kim, F. Blaabjerg, and A. Sangwongwanich, *Advances in Grid-Connected Photovoltaic Power Conversion Systems*. Woodhead Publishing, 2018.
- [10] S. A. M. Said, G. Hassan, H. M. Walwil, and N. Al-Aqeeli, “The effect of environmental factors and dust accumulation on photovoltaic modules and dust-accumulation mitigation strategies,” *Renewable and Sustainable Energy Reviews*, vol. 82, pp. 743–760, Feb. 2018.
- [11] M. M. Fouad, L. A. Shihata, and E. I. Morgan, “An integrated review of factors influencing the performance of photovoltaic panels,” *Renewable and Sustainable Energy Reviews*, vol. 80, pp. 1499–1511, Dec. 2017.
- [12] A. Dhaundiyal and D. Atsu, “Energy assessment of photovoltaic modules,” *Solar Energy*, vol. 218, pp. 337–345, Apr. 2021.
- [13] E. L. Meyer and E. E. van Dyk, “Assessing the Reliability and Degradation of Photovoltaic Module Performance Parameters,” *IEEE Transactions on Reliability*, vol. 53, no. 1, pp. 83–92, Mar. 2004.
- [14] M. Saidan, A. G. Albaali, E. Alasis, and J. K. Kaldellis, “Experimental study on the effect of dust deposition on solar photovoltaic panels in desert environment,” *Renewable Energy*, vol. 92, pp. 499–505, Jul. 2016.

- [15] A. A. Babatunde, S. Abbasoglu, and M. Senol, "Analysis of the impact of dust, tilt angle and orientation on performance of PV Plants," *Renewable and Sustainable Energy Reviews*, vol. 90, pp. 1017–1026, Jul. 2018.
- [16] A. Dolara, G. C. Lazaroiu, S. Leva, and G. Manzolini, "Experimental investigation of partial shading scenarios on PV (photovoltaic) modules," *Energy*, vol. 55, pp. 466–475, Jun. 2013.
- [17] P. Manganiello, M. Balato, and M. Vitelli, "A Survey on Mismatching and Aging of PV Modules: The Closed Loop," *IEEE Transactions on Industrial Electronics*, vol. 62, no. 11, pp. 7276–7286, Nov. 2015.
- [18] O. O. Ogbomo, E. H. Amalu, N. N. Ekere, and P. O. Olagbegi, "Effect of operating temperature on degradation of solder joints in crystalline silicon photovoltaic modules for improved reliability in hot climates," *Solar Energy*, vol. 170, pp. 682–693, Aug. 2018.
- [19] K. A. Kim and P. T. Krein, "Hot spotting and second breakdown effects on reverse I-V characteristics for mono-crystalline Si Photovoltaics," in *2013 IEEE Energy Conversion Congress and Exposition*, Sep. 2013, pp. 1007–1014.
- [20] S. Silvestre, A. Boronat, and A. Chouder, "Study of bypass diodes configuration on PV modules," *Applied Energy*, vol. 86, no. 9, pp. 1632–1640, Sep. 2009.
- [21] N. D. Kaushika and A. K. Rai, "An investigation of mismatch losses in solar photovoltaic cell networks," *Energy*, vol. 32, no. 5, pp. 755–759, May 2007.
- [22] F. Belhachat and C. Larbes, "A review of global maximum power point tracking techniques of photovoltaic system under partial shading conditions," *Renewable and Sustainable Energy Reviews*, vol. 92, pp. 513–553, Sep. 2018.
- [23] M. Nasir and M. F. Zia, "Global maximum power point tracking algorithm for photovoltaic systems under partial shading conditions," in *2014 16th International Power Electronics and Motion Control Conference and Exposition*, Sep. 2014, pp. 667–672.
- [24] Y.-H. Liu, C.-L. Liu, J.-W. Huang, and J.-H. Chen, "Neural-network-based maximum power point tracking methods for photovoltaic systems operating under fast changing environments," *Solar Energy*, vol. 89, pp. 42–53, Mar. 2013.
- [25] S. Daraban, D. Petreus, and C. Morel, "A novel MPPT (maximum power point tracking) algorithm based on a modified genetic algorithm specialized on tracking the global maximum power point in photovoltaic systems affected by partial shading," *Energy*, vol. 74, pp. 374–388, Sep. 2014.
- [26] Y. Jeon, H. Lee, K. A. Kim, and J. Park, "Least Power Point Tracking Method for Photovoltaic Differential Power Processing Systems," *IEEE Transactions on Power Electronics*, vol. 32, no. 3, pp. 1941–1951, Mar. 2017.
- [27] K. A. Kim and P. T. Krein, "Reexamination of Photovoltaic Hot Spotting to Show Inadequacy of the Bypass Diode," *IEEE Journal of Photovoltaics*, vol. 5, no. 5, pp. 1435–1441, Sep. 2015.
- [28] K. Kesarwani and J. T. Stauth, "A comparative theoretical analysis of distributed ladder converters for sub-module PV energy optimization," in *2012 IEEE 13th Workshop on Control and Modeling for Power Electronics (COMPEL)*, Jun. 2012, pp. 1–6.

- [29] H. J. Bergveld *et al.*, “Module-Level DC/DC Conversion for Photovoltaic Systems: The Delta-Conversion Concept,” *IEEE Transactions on Power Electronics*, vol. 28, no. 4, pp. 2005–2013, Apr. 2013.
- [30] L. F. Lavado Villa, T.-P. Ho, J.-C. Crebier, and B. Raison, “A Power Electronics Equalizer Application for Partially Shaded Photovoltaic Modules,” *IEEE Transactions on Industrial Electronics*, vol. 60, no. 3, pp. 1179–1190, Mar. 2013.
- [31] C. Olalla, D. Clement, M. Rodriguez, and D. Maksimovic, “Architectures and Control of Submodule Integrated DC–DC Converters for Photovoltaic Applications,” *IEEE Transactions on Power Electronics*, vol. 28, no. 6, pp. 2980–2997, Jun. 2013.
- [32] O. Khan and W. Xiao, “Review and qualitative analysis of submodule-level distributed power electronic solutions in PV power systems,” *Renewable and Sustainable Energy Reviews*, vol. 76, pp. 516–528, Sep. 2017.
- [33] M. Uno and T. Shinohara, “Module-Integrated Converter Based on Cascaded Quasi-Z-Source Inverter With Differential Power Processing Capability for Photovoltaic Panels Under Partial Shading,” *IEEE Transactions on Power Electronics*, vol. 34, no. 12, pp. 11553–11565, Dec. 2019.
- [34] H. Jeong, H. Lee, Y. Liu, and K. A. Kim, “Review of Differential Power Processing Converters Techniques for Photovoltaic Applications,” *IEEE Transactions on Energy Conversion*, vol. 34, no. 1, pp. 351–360, 2018.
- [35] P. S. Shenoy and P. T. Krein, “Differential Power Processing for DC Systems,” *IEEE Transactions on Power Electronics*, vol. 28, no. 4, pp. 1795–1806, Apr. 2013.
- [36] G. Chu, H. Wen, L. Jiang, Y. Hu, and X. Li, “Bidirectional flyback based isolated-port submodule differential power processing optimizer for photovoltaic applications,” *Solar Energy*, vol. 158, pp. 929–940, Dec. 2017.
- [37] W. Xiao, N. Ozog, and W. G. Dunford, “Topology Study of Photovoltaic Interface for Maximum Power Point Tracking,” *IEEE Transactions on Industrial Electronics*, vol. 54, no. 3, pp. 1696–1704, Jun. 2007.
- [38] D. Vinnikov, A. Chub, L. Liivik, R. Kosenko, and O. Korkh, “Solar Optiverter - A Novel Hybrid Approach to the Photovoltaic Module Level Power Electronics,” *IEEE Transactions on Industrial Electronics*, pp. 1–1, 2018.
- [39] A. S. Rana, M. Nasir, and H. A. Khan, “String level optimisation on grid-tied solar PV systems to reduce partial shading loss,” *IET Renewable Power Generation*, vol. 12, no. 2, pp. 143–148, Nov. 2017.
- [40] M. K. Alam, F. Khan, J. Johnson, and J. Flicker, “A Comprehensive Review of Catastrophic Faults in PV Arrays: Types, Detection, and Mitigation Techniques,” *IEEE Journal of Photovoltaics*, vol. 5, no. 3, pp. 982–997, May 2015.
- [41] G. R. Walker and P. C. Sernia, “Cascaded DC-DC converter connection of photovoltaic modules,” *IEEE Transactions on Power Electronics*, vol. 19, no. 4, pp. 1130–1139, Jul. 2004.
- [42] S. M. MacAlpine, R. W. Erickson, and M. J. Brandemuehl, “Characterization of Power Optimizer Potential to Increase Energy Capture in Photovoltaic Systems

- Operating Under Nonuniform Conditions,” *IEEE Transactions on Power Electronics*, vol. 28, no. 6, pp. 2936–2945, Jun. 2013.
- [43] P. S. Shenoy, K. A. Kim, B. B. Johnson, and P. T. Krein, “Differential Power Processing for Increased Energy Production and Reliability of Photovoltaic Systems,” *IEEE Transactions on Power Electronics*, vol. 28, no. 6, pp. 2968–2979, Jun. 2013.
- [44] P. S. Shenoy, K. A. Kim, P. T. Krein, and P. L. Chapman, “Differential power processing for efficiency and performance leaps in utility-scale photovoltaics,” in *2012 38th IEEE Photovoltaic Specialists Conference*, Jun. 2012.
- [45] M. Tahmasbi-Fard, M. Tarafdar-Hagh, S. Pourpayam, and A. Haghrah, “A Voltage Equalizer Circuit to Reduce Partial Shading Effect in Photovoltaic String,” *IEEE Journal of Photovoltaics*, vol. 8, no. 4, pp. 1102–1109, Jul. 2018.
- [46] M. Z. Ramli and Z. Salam, “A Simple Energy Recovery Scheme to Harvest the Energy from Shaded Photovoltaic Modules During Partial Shading,” *IEEE Transactions on Power Electronics*, vol. 29, no. 12, pp. 6458–6471, Dec. 2014.
- [47] J. T. Stauth, M. D. Seeman, and K. Kesarwani, “Resonant Switched-Capacitor Converters for Sub-module Distributed Photovoltaic Power Management,” *IEEE Transactions on Power Electronics*, vol. 28, no. 3, pp. 1189–1198, Mar. 2013.
- [48] M. Uno and A. Kukita, “PWM Switched Capacitor Converter With Switched-Capacitor-Inductor Cell for Adjustable High Step-Down Voltage Conversion,” *IEEE Transactions on Power Electronics*, vol. 34, no. 1, pp. 425–437, Jan. 2019.
- [49] M. Gokdag, M. Akbaba, and O. Gulbudak, “Switched-capacitor converter for PV modules under partial shading and mismatch conditions,” *Solar Energy*, vol. 170, pp. 723–731, Aug. 2018.
- [50] M. Uno, Y. Saito, S. Urabe, and M. Yamamoto, “PWM Switched Capacitor-Based Cell-Level Power Balancing Converter Utilizing Diffusion Capacitance of Photovoltaic Cells,” *IEEE Transactions on Power Electronics*, vol. 34, no. 11, pp. 10675–10687, Nov. 2019.
- [51] M. Uno, M. Yamamoto, H. Sato, and S. Oyama, “Modularized Differential Power Processing Architecture Based on Switched Capacitor Converter to Virtually Unify Mismatched Photovoltaic Panel Characteristics,” *IEEE Transactions on Power Electronics*, vol. 35, no. 2, pp. 1563–1575, Feb. 2020.
- [52] A. Blumenfeld, A. Cervera, and M. M. Peretz, “Enhanced Differential Power Processor for PV Systems: Resonant Switched-Capacitor Gyrator Converter With Local MPPT,” *IEEE Journal of Emerging and Selected Topics in Power Electronics*, vol. 2, no. 4, pp. 883–892, Dec. 2014.
- [53] S. Ben-Yaakov, A. Cervera, A. Blumenfeld, and M. M. Peretz, “Resonant switched-capacitor gyrator-type converter with local MPPT capability for PV cells,” US9906189B2, Feb. 27, 2018.
- [54] J. T. Stauth, M. D. Seeman, and K. Kesarwani, “A Resonant Switched-Capacitor IC and Embedded System for Sub-Module Photovoltaic Power Management,” *IEEE Journal of Solid-State Circuits*, vol. 47, no. 12, pp. 3043–3054, Dec. 2012.

- [55] A. H. Chang, A. Avestruz, and S. B. Leeb, "Capacitor-Less Photovoltaic Cell-Level Power Balancing using Diffusion Charge Redistribution," *IEEE Transactions on Power Electronics*, vol. 30, no. 2, pp. 537–546, Feb. 2015.
- [56] C. Pascual and P. T. Krein, "Switched capacitor system for automatic series battery equalization," in *Proceedings of APEC 97 - Applied Power Electronics Conference*, Feb. 1997, vol. 2, pp. 848–854 vol.2.
- [57] M. Uno, H. Sato, and T. Ishikawa, "Differential Power Processing Converter Enhancing Energy Yield of Curved Solar Roofs of Plug-in Hybrid Electric Vehicles," *IEEE Transactions on Vehicular Technology*, vol. 69, no. 12, 14689 - 14700, 2020.
- [58] M. S. Zaman *et al.*, "A Cell-Level Differential Power Processing IC for Concentrating-PV Systems With Bidirectional Hysteretic Current-Mode Control and Closed-Loop Frequency Regulation," *IEEE Transactions on Power Electronics*, vol. 30, no. 12, pp. 7230–7244, Dec. 2015.
- [59] Y. Levron, D. R. Clement, B. Choi, C. Olalla, and D. Maksimovic, "Control of Submodule Integrated Converters in the Isolated-Port Differential Power-Processing Photovoltaic Architecture," *IEEE Journal of Emerging and Selected Topics in Power Electronics*, vol. 2, no. 4, pp. 821–832, Dec. 2014.
- [60] D. La Manna, V. Li Vigni, E. Riva Sanseverino, V. Di Dio, and P. Romano, "Reconfigurable electrical interconnection strategies for photovoltaic arrays: A review," *Renewable and Sustainable Energy Reviews*, vol. 33, pp. 412–426, May 2014.
- [61] P. R. Satpathy, S. Jena, and R. Sharma, "Power enhancement from partially shaded modules of solar PV arrays through various interconnections among modules," *Energy*, vol. 144, pp. 839–850, Feb. 2018.
- [62] P. R. Satpathy, S. Jena, B. Jena, and R. Sharma, "Comparative study of interconnection schemes of modules in solar PV array network," in *2017 International Conference on Circuit ,Power and Computing Technologies (ICCPCT)*, Apr. 2017, pp. 1–6.
- [63] A. S. Yadav, R. K. Pachauri, Y. K. Chauhan, S. Choudhury, and R. Singh, "Performance enhancement of partially shaded PV array using novel shade dispersion effect on magic-square puzzle configuration," *Solar Energy*, vol. 144, pp. 780–797, Mar. 2017.
- [64] G. Velasco-Quesada, F. Guinjoan-Gispert, R. Pique-Lopez, M. Roman-Lumbreras, and A. Conesa-Roca, "Electrical PV Array Reconfiguration Strategy for Energy Extraction Improvement in Grid-Connected PV Systems," *IEEE Transactions on Industrial Electronics*, vol. 56, no. 11, pp. 4319–4331, Nov. 2009.
- [65] G. Sai Krishna and T. Moger, "Reconfiguration strategies for reducing partial shading effects in photovoltaic arrays: State of the art," *Solar Energy*, vol. 182, pp. 429–452, Apr. 2019.
- [66] S. R. Pendem, S. Mikkili, and P. K. Bonthagorla, "PV Distributed-MPP Tracking: Total-Cross-Tied Configuration of String-Integrated-Converters to

- Extract the Maximum Power Under Various PSCs,” *IEEE Systems Journal*, vol. 14, no. 1, pp. 1046–1057, Mar. 2020.
- [67] N. D. Kaushika and N. K. Gautam, “Energy yield simulations of interconnected solar PV arrays,” *IEEE Transactions on Energy Conversion*, vol. 18, no. 1, pp. 127–134, Mar. 2003.
- [68] P. R. Satpathy, R. Sharma, and S. Jena, “A shade dispersion interconnection scheme for partially shaded modules in a solar PV array network,” *Energy*, vol. 139, pp. 350–365, Nov. 2017.
- [69] S. Malathy and R. Ramaprabha, “Reconfiguration strategies to extract maximum power from photovoltaic array under partially shaded conditions,” *Renewable and Sustainable Energy Reviews*, vol. 81, pp. 2922–2934, Jan. 2018.
- [70] B. Dhanalakshmi and N. Rajasekar, “A novel Competence Square based PV array reconfiguration technique for solar PV maximum power extraction,” *Energy Conversion and Management*, vol. 174, pp. 897–912, Oct. 2018.
- [71] M. Horoufiany and R. Ghandehari, “Optimization of the Sudoku based reconfiguration technique for PV arrays power enhancement under mutual shading conditions,” *Solar Energy*, vol. 159, pp. 1037–1046, Jan. 2018.
- [72] M. Premkumar, U. Subramaniam, T. S. Babu, R. M. Elavarasan, and L. Mihet-Popa, “Evaluation of Mathematical Model to Characterize the Performance of Conventional and Hybrid PV Array Topologies under Static and Dynamic Shading Patterns,” *Energies*, vol. 13, no. 12, Art. no. 12, Jan. 2020.
- [73] F. Flores-Bahamonde, J. Rojas, S. Kouro, A. M. Llor, C. A. Rojas, and M. A. Perez, “Sub-modular Power Optimizers Based on Partial Power Converters for Utility Scale PV Plants,” in *IECON 2019 - 45th Annual Conference of the IEEE Industrial Electronics Society*, Oct. 2019, vol. 1, pp. 4423–4428.



## **Selected Publications**

ISSN (online): 2446-1636  
ISBN (online): 978-87-7210-962-6

AALBORG UNIVERSITY PRESS